Influence of molecular transport on burning rate and conditioned species concentrations in highly turbulent premixed flames

Influence of molecular transport on burning rate and conditioned species concentrations in highly turbulent premixed flames

H. C. Lee[1,2],P. Dai[1], M. Wan[1,2], †, A. N. Lipatnikov[3],‡

[1]Guangdong Provincial Key Laboratory of Turbulence Research and Applications, Department of Mechanics and Aerospace Engineering, Southern University of Science and Technology, Shenzhen 518055, China

[2]Guangdong-Hong Kong-Macao Joint Laboratory for Data-Driven Fluid Mechanics and Engineering Applications, Southern University of Science and Technology, Shenzhen 518055, China

[3]Department of Mechanics and Maritime Sciences, Chalmers University of Technology, Gothenburg, 412 96, Sweden

(Received 1 September 2021)

Apparent inconsistency between (i) experimental and Direct Numerical Simulation (DNS) data that show the significant influence of differential diffusion on turbulent burning rate and (ii) recent complex-chemistry DNS data that indicate mitigation of the influence of differential diffusion on conditioned profiles of various local flame characteristics at high Karlovitz numbers is explored by analyzing new DNS data obtained from lean hydrogen-air turbulent flames. Both aforementioned effects are observed by analyzing the same DNS data provided that the conditioned profiles are sampled from the entire computational domain. On the contrary, the conditioned profiles sampled at the leading edge of the mean flame brush do not indicate the mitigation, but are significantly affected by differential diffusion phenomena, e.g., because reaction zones are highly curved at the leading edge. This observation is consistent with a significant increase in the computed turbulent burning velocity with decreasing Lewis number, with all the results considered jointly being consonant with the leading point concept of premixed turbulent combustion. The concept is further supported by comparing DNS data obtained by allowing for preferential diffusion solely for a single species, either atomic or molecular hydrogen.

Key words: differential diffusion, Lewis number, flame speed, burning velocity, DNS

1. Introduction

Rapidly growing interest in utilizing chemical energy bound in renewable carbon-free fuels such as hydrogen highlights a fundamental challenge that has not yet received proper attention. The challenge consists in understanding and modeling strong differential diffusion effects in turbulent premixed flames. More specifically, difference between molecular diffusivities of reactants or between the Lewis number $Le = D/\kappa$ and unity is well known to substantially affect burning rate even in intense turbulence (Lipatnikov 2012), with such effects being especially pronounced in lean hydrogen-air flames due to a high diffusivity of H_2. Here, D and κ are molecular diffusivity of a deficient reactant (e.g.,

† Email address for correspondence: wanmp@sustech.edu.cn
‡ Email address for correspondence: lipatn@chalmers.se

the fuel in a lean mixture) and molecular heat diffusivity of the mixture, respectively. For instance, significant influence of the aforementioned differences on turbulent flame speed S_t was documented in experiments by Wohl & Shore (1955), Karpov & Sokolik (1961); Karpov & Severin (1980), Abdel-Gayed et al. (1984a), Kido et al. (1989), Wu et al. (1990), and in many other measurements reviewed elsewhere (Kuznetsov & Sabelnikov 1990; Lipatnikov & Chomiak 2005). Recently, an extremely high magnitude of such differential diffusion effects was reported by Yang et al. (2018).

From the qualitative perspective, the discussed effects are known to stem from variations in the local temperature and mixture composition due to imbalance of reactant and heat fluxes to/from thin reaction zones strained and curved by turbulent eddies (Bradley et al. 1992; Kuznetsov & Sabelnikov 1990; Lipatnikov 2012; Lipatnikov & Chomiak 2005). Similar effects are predicted by theories of laminar premixed flames stretched by large-scale flow perturbations (Class et al. 2003; Kelley et al. 2012; Matalon & Matkowsky 1982; Pelcé & Clavin 1982; Zel'dovich et al. 1985), but these theories are rigorous for weak perturbations of the local flame speed only. However, the problem of predicting a strong increase in the turbulent burning rate due to differential diffusion has not yet been solved. On the contrary, the vast majority of numerical models of premixed turbulent combustion, discussed in widely cited books (Peters 2000; Poinsot & Veynante 2005) and review papers (Bilger et al. 2005; Veynante & Vervisch 2002), disregard the influence of differences in molecular transport coefficients on S_t.

While rapid progress in Direct Numerical Simulation (DNS) of turbulent reacting flows has been yielding new opportunities for model development, recent DNS data do not seem to clarify understanding of the differential diffusion effects in highly turbulent premixed flames. Vice versa, on the one hand, a significant influence of differences in molecular transport coefficients on bulk and/or local burning rates was documented in single-step-chemistry (Chakraborty & Cant 2011; Chakraborty & Lipatnikov 2013a,b; Chakraborty et al. 2016) and complex-chemistry (Aspden et al. 2019; Lapointe & Blanquart 2016; Lapointe et al. 2015; Rieth et al. 2021; Savard et al. 2015; Wiseman et al. 2021) DNS studies. On the other hand, recent DNS studies (Aspden et al. 2011a,b, 2016, 2019; Lapointe et al. 2015; Savard & Blanquart 2014; Savard et al. 2015) have shown that, with increasing Karlovitz number Ka, conditioned profiles of various local mixture characteristics, e.g., the equivalence ratio, sampled from highly turbulent flames, tend to the counterpart profiles computed for the unity Lewis number unperturbed laminar flame.

These two apparently inconsistent findings do not necessarily contradict each other, e.g., both findings were reported by analyzing the same DNS data in the same papers (Aspden et al. 2019; Lapointe et al. 2015; Savard et al. 2015). Nevertheless, the latter finding (conditioned profiles) is often interpreted to evidence that "differential diffusion disappears when the turbulent diffusivity greatly exceeds the molecular diffusivity" (Driscoll et al. 2020, p. 21) or "local phenomena such as differential diffusion become less important in a statistical sense" at high Ka (Nilsson et al. 2018, p. 628). Such an interpretation is further prompted by (i) a suggestion to model highly turbulent flames by using an "effective Lewis number" that involves turbulent Reynolds number Re_t and tends to unity as $Re_t \to \infty$ (Savard & Blanquart 2014; Savard et al. 2015) and (ii) DNS data that indicate that, with increasing Ka, conditioned profiles of fuel consumption and heat release rates, sampled from the entire flame brush, approach the counterpart profiles obtained from the unity Lewis number unperturbed laminar flame (Lapointe et al. 2015, figures 8 and 9). However, the present authors are not aware on an experimental study that shows mitigation of the influence of differential diffusion on turbulent burning rate with increasing Ka, whereas a well pronounced influence was documented at very high Karlovitz (Karpov & Severin 1980; Yang et al. 2018) or Reynolds (Daniele et al. 2011;

Wu et al. 1990) numbers, as well as at high ratios $u'/S_L = O(100)$ (Venkateswaran et al. 2011, 2013) of the rms turbulent velocity u' to the laminar flame speed S_L.

While consistency of the two discussed findings appears to be of significant fundamental and applied interest, the present authors are not aware on a target-directed research into this issue. Even if both findings were reported in the same DNS papers (Aspden et al. 2019; Lapointe et al. 2015; Savard et al. 2015), discussion of their consistency was brief (if any) and their coexistence seems to be indirectly attributed to insufficiently high Karlovitz numbers. The goal of the present communication is to bridge this knowledge gap by analyzing recent DNS data that show both findings.

The DNS attributes are summarized in the next section. Numerical results are reported and discussed in section 3, followed by concluding remarks.

2. DNS attributes

Three-dimensional simulations of statistically one-dimensional and planar †, lean (the equivalence ratio $\phi = 0.5$) hydrogen-air premixed flames propagating in forced turbulence under the room conditions were performed employing the solver DINO (Abdelsamie et al. 2016). It involves a 6th-order finite-difference central stencil and a semi-implicit 3rd-order Runge–Kutta method for time integration in order to numerically solve the low-Mach-number formulation of the Navier-Stokes equations, as well as energy and species transport equations where chemical kinetics and mixture-averaged molecular transport are modeled using open-source library Cantera-2.3 (Goodwin et al. 2009). A detailed chemical mechanism (9 species and 22 reversible reactions) by Kéromnès et al. (2013) was adopted in the simulations.

A rectangular computational domain of $\Lambda \times \beta\Lambda \times \Lambda$, where $\Lambda = 2.4$ mm, was discretized using a uniform Cartesian grid of $N \times \beta N \times N$ cells. The values of N are reported in table 1, with $\beta = 18$ in cases A, B, A1, and B1 and $\beta = 16$ in other four cases. Periodic boundary conditions were imposed along the x and z directions and inflow and outflow boundary conditions were set along the streamwise y direction.

At the inlet, the rms velocity was equal to 0.05 m/s, with turbulence being generated using the linear velocity forcing method (Carroll & Blanquart 2014; Lundgren 2003; Rosales & Meneveau 2005) between $y = 0.5\Lambda$ and $y = 8\Lambda$. In the beginning of each case, constant-density turbulence was simulated for at least $50\tau_t$. Here, $\tau_t = L/u'$ is eddy turnover time and the integral length scale L is approximately equal to 0.19Λ (Carroll & Blanquart 2014; Lundgren 2003; Rosales & Meneveau 2005). Turbulence generation and forcing methods used in the present study, as well as turbulence characteristics within the flame brushes, are discussed in a more detail manner elsewhere (Lee et al. 2021a).

Subsequently, the steady unperturbed laminar flame solution yielded by Cantera-2.3 (Goodwin et al. 2009) was embedded into the flow field, followed by the flame propagation along the y-axis from right to left. When necessary, the mean inlet velocity was adjusted in order to retain the flame within the forced-flow subdomain where the transverse-averaged turbulent kinetic energy varied weakly along the y-axis or in time (Lee et al. 2021a, figure 2). As a result, the flame brush never approached the inlet boundary, with the distance between the flame leading edge and the boundary being always larger than 0.5Λ.

The combustion simulations were performed for at least $28\tau_t$. Time-dependent mean quantities $\langle q \rangle(y,t)$ were evaluated by averaging the field $q(\boldsymbol{x},t)$ over transverse plane

† Effects discussed in the following could be more pronounced in statistically curved turbulent flames, which are more common in applications.

Case	S_L, m/s	δ_L, mm	u'/S_L	L/δ_L	Re_t	Ka	Da	$\Delta x/L$	$\Delta x/\eta$	N	$\bar{U}_t^F/S_L$	$\bar{U}_t^T/S_L$	$\bar{U}_t^F$ m/s	$\bar{U}_t^T$ m/s
A	0.58	0.41	2.2	1.1	30	3.0	0.53	0.082	1.08	64	4.1	4.0	2.4	2.35
B	0.58	0.41	4.0	1.1	56	9.0	0.29	0.055	1.13	96	5.4	5.3	3.1	3.1
C	0.58	0.41	11.8	1.1	158	33.0	0.10	0.041	1.85	128	8.9	8.6	5.2	5.0
A1	0.78	0.29	1.6	1.6	30	1.6	1.0	0.082	1.08	64	2.7	2.6	2.1	2.0
B1	0.78	0.29	3.0	1.6	56	4.0	0.54	0.055	1.13	96	3.2	3.0	2.5	2.4
C1	0.78	0.29	8.3	1.6	158	19.0	0.19	0.041	1.85	128	4.3	4.1	3.35	3.3
C1/H	0.91	0.34	7.1	1.4	158	16.6	0.19	0.041	1.85	128	2.8	2.8	2.6	2.5
C1/H2	0.51	0.34	12.7	1.4	158	39.4	0.10	0.041	1.85	128	12.6	12.0	6.4	6.1

TABLE 1. Characteristic parameters of DNS cases.

y =const. Statistically stationary mean quantities $\bar{q}(y)$ were computed by averaging $\langle q \rangle(y,t)$ over time at $t/\tau_t > t^*$, where $t^* = 6$, 10, and 15 in cases A, B, and C, respectively, see vertical dashed lines in figure 1. The combustion progress variable was defined using the fuel mass fraction, i.e., $c = (Y_{H_2,u} - Y_{H_2})/Y_{H_2,u}$. The local equivalence ratio ϕ, flame curvature h_m, and strain rate a_t were calculated as follows:

$$\phi = \frac{1}{2}\frac{2X_{H_2} + 2X_{H_2O} + X_H + X_{OH} + X_{HO_2} + 2X_{H_2O_2}}{2X_{O_2} + X_{H_2O} + X_O + X_{OH} + 2X_{HO_2} + 2X_{H_2O_2}}, \tag{2.1}$$

$$h_m = \frac{1}{2}\nabla \cdot \boldsymbol{n}, \tag{2.2}$$

$$a_t = -\boldsymbol{n}\boldsymbol{n} : \nabla \boldsymbol{u} + \nabla \cdot \boldsymbol{u}. \tag{2.3}$$

Here, $\boldsymbol{n} = -\nabla c/|\nabla c|$ is the unit normal vector and, consequently, the curvature is positive when its center is in combustion products, $\boldsymbol{u}$ designates the flow velocity field, and X_k is the mole fraction of species k.

The simulation conditions are reported in table 1, where $\delta_L = (T_b - T_u)/\max\{|dT/dx|\}$ and $\tau_f = \delta_L/S_L$ are the laminar flame thickness and time scale, respectively; $Da = \tau_t/\tau_f$, $Ka = (u'/S_L)^{3/2}(\delta_L/L)^{1/2}$, and $Re_t = u'L/\nu_u$ are the Damköhler, Karlovitz, and turbulent Reynolds numbers, respectively; T is the temperature; ν_u is the kinematic viscosity of unburned mixture; Δx is the grid size; $\eta = LRe_t^{-3/4}$ is the Kolmogorov length scale; subscripts u and b designate unburned and burned fluid, respectively.

Cases A, B, and C are characterized by (i) a low Lewis number $Le = 0.32$ and (ii) different rms velocities u', which are increased from case A to case C. Cases A1, B1, and C1 correspond to cases A, B, and C, respectively, with molecular diffusivities being set equal to κ for each species. Thus, $Le = 1$ in cases A1, B1, and C1. Since an increase in Le results in increasing the unperturbed laminar flame speed (Zel'dovich et al. 1985), Damköhler or Karlovitz numbers are different in each pair of the considered cases. Cases C1/H and C1/H2 are intermediate between cases C and C1, i.e., molecular diffusivities of all species with the exception of H and H_2, respectively, are equal to κ, as in case C1, whereas molecular diffusivity of H or H_2 is equal to its mixture-averaged value used in case C.

The adopted numerical meshes ensure 11 grid points across the thickness δ_L in cases A, A1, B, and B1 and more than 20 grid points in cases C, C1, C1/H, and C1/H2 characterized by the highest Karlovitz numbers. In all cases, the Kolmogorov length scale is greater than half the grid size, thus, indicating acceptable resolution of the turbulent flow (Yeung & Pope 1989).

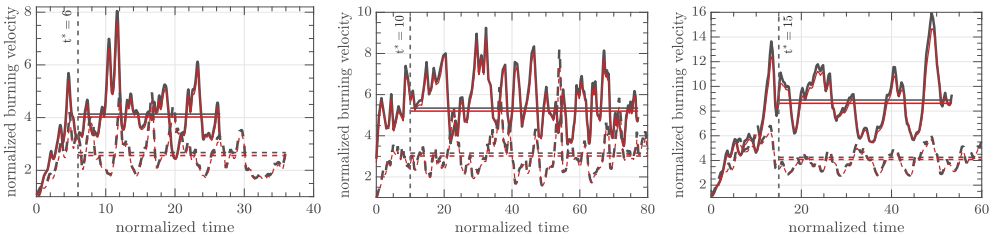

FIGURE 1. Evolution of the normalized turbulent burning velocities U_t^F/S_L (red lines) and U_t^T/S_L (black lines) in flames (a) A and A1, (b) B and B1, (c) C and C1. Results obtained from low and unity Lewis number flames are plotted in solid and dashed lines, respectively. Horizontal straight lines show mean values.

In addition to the DNS of turbulent flames, stationary laminar flames were simulated using the same chemical mechanism (Kéromnès et al. 2013) and open-access code Cantera (Goodwin et al. 2009). Such computations were performed for unperturbed flames in cases of $Le = 0.32$ and $Le = 1$ and for planar one-dimensional counterflow flames at different strain rates. The counterflow flames were used for comparison following common practice (Amato et al. 2015a,b; Aspden et al. 2011a,b, 2019; Driscoll et al. 2020; Lapointe & Blanquart 2016; Lapointe et al. 2015; Savard & Blanquart 2014; Savard et al. 2015; Venkateswaran et al. 2011, 2013; Zhang et al. 2018).

3. Results and discussion

3.1. *Turbulent burning velocities and conditioned profiles*

Figure 1 reports evolution of turbulent burning velocities (i) $U_t^F(t)$ evaluated by integrating the fuel consumption rate $\dot{\omega}_{H_2}(\boldsymbol{x}, t)$ over the computational domain, i.e.,

$$U_t^F(t) = -\frac{1}{(\rho Y_{H_2})_u \Lambda^2} \iiint \dot{\omega}_{H_2}(\boldsymbol{x}, t) d\boldsymbol{x}, \tag{3.1}$$

or (ii) $U_t^T(t)$ obtained by integrating the heat release rate $\dot{\omega}_T(\boldsymbol{x}, t) = \sum_{k=1}^{N_{sp}} h_k \dot{\omega}_k(\boldsymbol{x}, t)$ over the computational domain, i.e.,

$$U_t^T(t) = \frac{1}{\Lambda^2} \iiint \frac{\dot{\omega}_T(\boldsymbol{x}, t)}{c_p(T_b - T_u)} d\boldsymbol{x}. \tag{3.2}$$

Here, ρ and Y designate density and mass fraction, respectively; h_k and $\dot{\omega}_k$ are the enthalpy and the rate of production, respectively, of species k; c_p is the heat capacity of the mixture; and $N_{sp} = 9$ is the number of species. These results have been obtained from flames (a) A and A1, (b) B and B1, (c) C and C1. Results computed in cases C1/H and C1/H2 will be discussed later.

After an initial stage, each computed curve oscillates around a mean value of U_t^F/S_L or U_t^T/S_L, see horizontal straight lines in figure 1. These mean values averaged at $t/\tau_t > t^*$ and the dimensional mean values of U_t^F and U_t^T are reported in table 1. The results obtained for U_t^F and U_t^T are close to one another, thus, indicating that fuel consumption and heat release are in an equilibrium state on the global level, as expected. However, such an equilibrium state is not observed on the local level, as will be discussed later.

Figure 1 and table 1 show that, in line with numerous experimental and DNS data discussed in the introduction, the present simulations do predict a significant increase

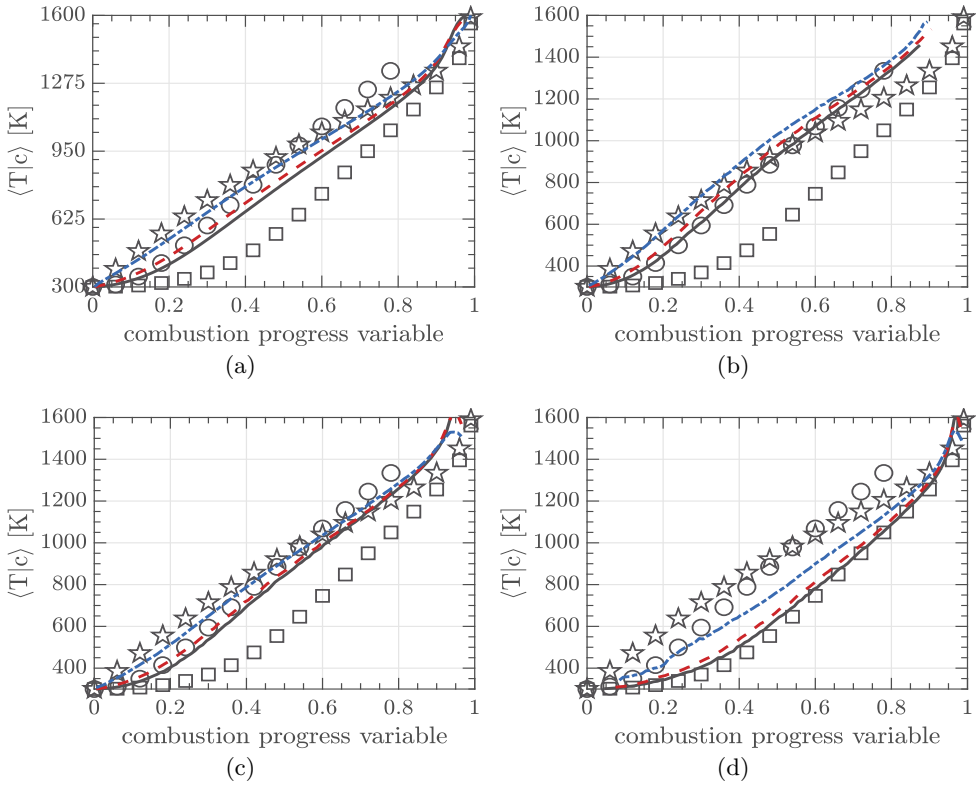

FIGURE 2. Time-averaged conditioned profiles of temperature extracted (a) from the entire computational domain, and at (b) $\langle c_F \rangle = 0.1 \pm 0.02$, ($c$) $\langle c_F \rangle = 0.5 \pm 0.02$, ($d$) $\langle c_F \rangle = 0.9 \pm 0.02$. Results computed in cases A, B, and C are plotted using black solid, red dashed, and blue dotted-dashed lines, respectively. Squares, pentagons, and circles show profiles computed for the unperturbed laminar low Lewis number flame, the unperturbed laminar unity Lewis number flame, and critically strained (the strain rate is equal to $11.3/\tau_f$), planar, stationary laminar low Lewis number flame, respectively.

in U_t^F/S_L or U_t^T/S_L with decreasing Le. It is of interest to note that the effect magnitude is increased by Ka under conditions of the present study. Indeed, a ratio of $(U_t^F/S_L)_{Le<1}/(U_t^F/S_L)_{Le=1}$ is equal to 1.5, 1.7, and 2.1 in the A, B, and C, respectively, pairs of flames. Thus, the computed bulk turbulent burning velocities do not indicate that molecular transport is dominated by turbulent mixing in the studied flames.

On the contrary, the conditioned profiles of the temperature, equivalence ratio, fuel consumption rate, heat release rate, and species mass fractions, e.g., mass fraction of the radical H, extracted from the entire computational domain at $t/\tau_t > t^*$ and plotted in figures 2(a), 3(a), 4(a), 5(a), and 6(a), respectively, suggest the opposite conclusion, i.e., molecular transport is dominated by turbulent mixing at least in case C characterized by the highest Karlovitz number. Indeed, in this case, the conditioned profiles of $\langle T|c\rangle(c)$, $\langle \phi|c\rangle(c)$, $\langle \dot{\omega}_{H_2}|c\rangle(c)$, $\langle \dot{\omega}_T|c\rangle(c)$, and $\langle Y_H|c\rangle(c)$, see blue dotted-dashed lines, differ significantly from the counterpart profiles obtained from the unperturbed, see squares, or highly strained, see circles, stationary planar laminar premixed flames characterized by $Le = 0.32$. However, the conditioned profiles are sufficiently close to the counterpart profiles obtained from the unperturbed unity Lewis number flame, see pentagons. In particular, the profiles of $\langle \dot{\omega}_{H_2}|c\rangle(c)$ are very close in the low Lewis number turbulent flame

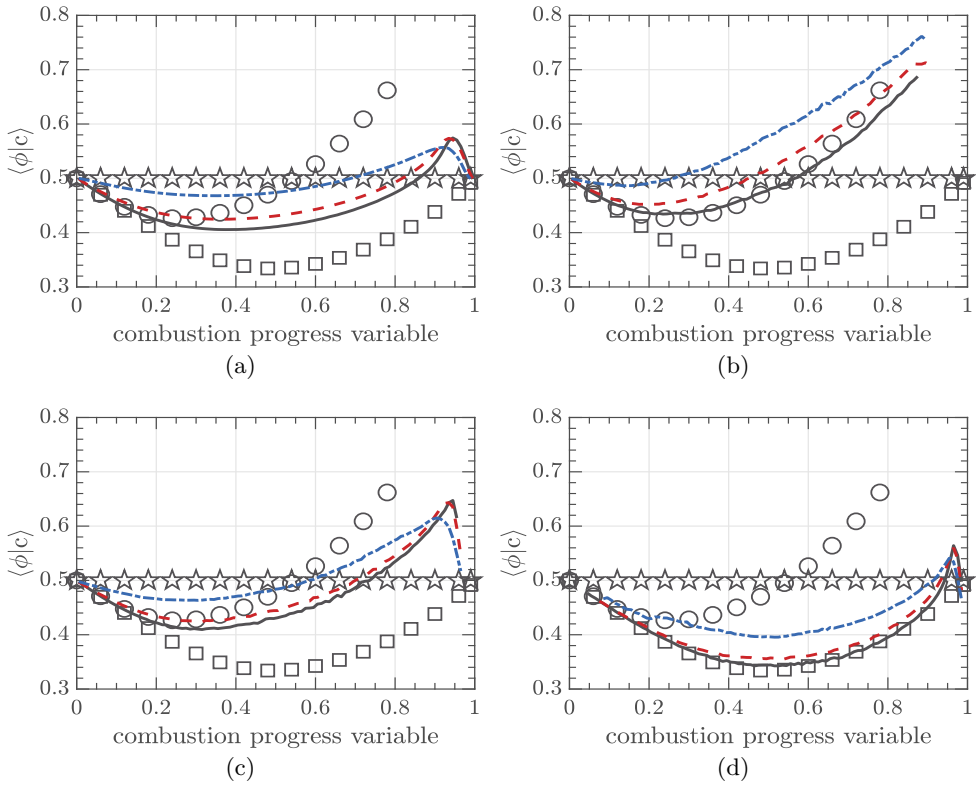

FIGURE 3. Time-averaged conditioned profiles of equivalence ratio. Legends are explained in caption to figure 2.

C and in the unity Lewis number unperturbed laminar flame, cf. blue dotted-dashed line and pentagons in figure 4(a). Even in cases B and A, the conditioned profiles are closer to the laminar-flame profiles computed for $Le = 1$ when compared to the low Lewis number flame profiles.

It is worth remembering that if Le is increased from 0.32 to 1.0, S_L is also increased, see table 1. Such an effect might be assumed to cause a higher U_t if molecular transport associated with a low Lewis number for lean hydrogen-air flames is dominated by turbulent mixing associated with $Le = 1$. However, the last two columns in table 1 show that the dimensional $\bar{U}_t^F$ or $\bar{U}_t^T$ is significantly higher in case C when compared to case C1 characterized by a larger S_L. Therefore, the high $\bar{U}_t^F$ or $\bar{U}_t^T$ in case C should not be attributed to an increase from $S_L(Le = 0.32) = 0.58$ m/s to $S_L(Le = 1.0) = 0.78$ m/s.

Thus, the DNS data involve both findings emphasized in the introduction and, consequently, are suitable for exploring their consistency, e.g., consistency of figure 1, which shows a significant influence of differential diffusion on the integrated fuel consumption or heat release rate, and figure 4(a) or 5(a), which shows that the conditioned fuel consumption rate $\langle \dot{\omega}_{H_2} | c \rangle (c)$ or heat release rate $\langle \dot{\omega}_T | c \rangle (c)$, respectively, sampled from the entire flame brush in case C approaches $\dot{\omega}_{H_2}(c)$ or $\dot{\omega}_T(c)$, respectively, in the unperturbed unity Lewis number laminar flame.

The apparent inconsistency between the DNS results plotted in figure 1 and figures 2(a), 3(a), 4(a), 5(a), and 6(a) is explained in other subfigures 2-6, where conditioned profiles extracted from (b) leading, (c) median, and (d) trailing layers of the mean flame

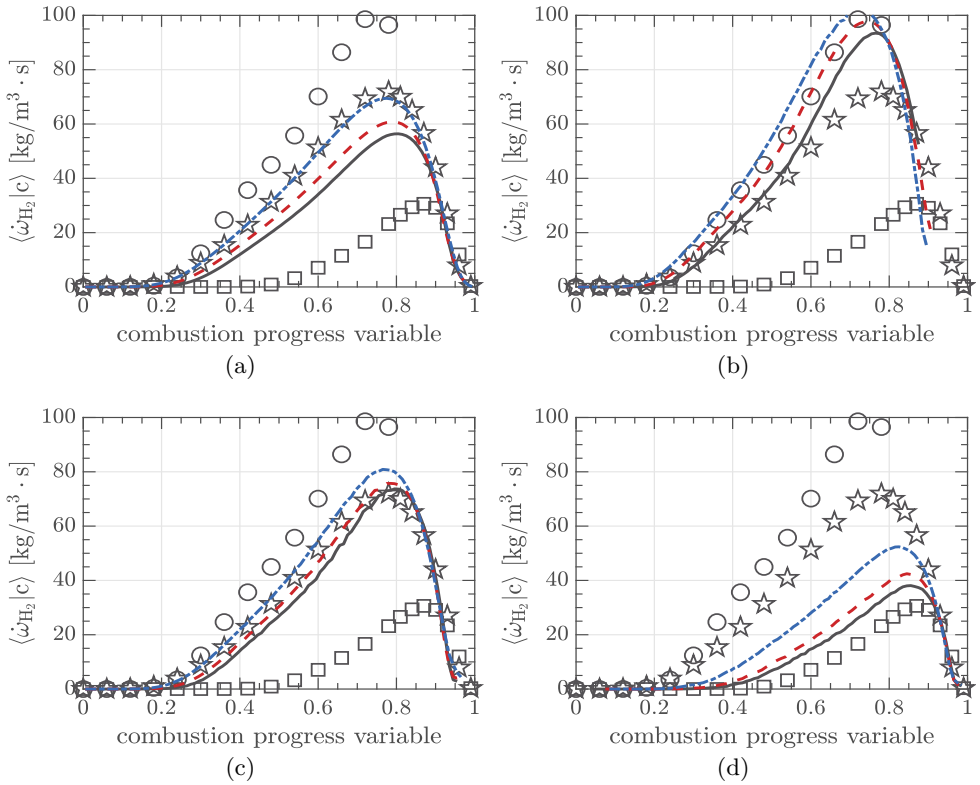

FIGURE 4. Time-averaged conditioned profiles of fuel consumption rate. Legends are explained in caption to figure 2.

brushes are reported. These three layers are characterized by the transverse-averaged combustion progress variable $\langle c \rangle(y,t)$ about (± 0.02) 0.1, 0.5, and 0.9, respectively. While the median conditioned profiles plotted in figures 2(c), 3(c), 4(c), 5(c), and 6(c) look similar to the conditioned profiles sampled from the entire computational domain, this is not so for the leading or trailing conditioned profiles. More specifically, the conditioned profiles (with the exception of $\langle \dot{\omega}_T | c \rangle$ in case C) sampled from the trailing layer are closer to the counterpart conditioned profiles obtained from the unperturbed low Lewis number laminar flame, cf. lines and squares in figures 2(d), 3(d), 4(d), 5(d), and 6(d). On the contrary, the conditioned profiles of $\langle \phi | c \rangle(c)$, $\langle \dot{\omega}_{H_2} | c \rangle$, and $\langle Y_H | c \rangle$ sampled from the leading layer are closer† to the counterpart conditioned profiles obtained from the highly strained low Lewis number laminar flame, cf. lines and circles in figures 3(b), 4(b), and 6(b). It is also worth stressing that the peak fuel consumption rate evaluated at $\langle c \rangle = 0.1 \pm 0.02$ is significantly higher than the peak rates in the unperturbed laminar flames (both $Le = 0.32$ and $Le = 1.0$), but is close to the peak rate in the highly strained low Lewis number laminar flame. Thus, under conditions of the present simulations, apparent dominance of turbulent mixing, implied by the results shown in figures 2(a), 3(a), 4(a), 5(a), and 6(a) is an artifact of sampling statistics from the entire computational

† For temperature, this trend is only pronounced at $c > 0.7$, cf. lines and circles in figure 2(b), whereas the profiles of $T(c)$ obtained from the unperturbed unity Lewis number and highly strained low Lewis number laminar flames are close to one another at $c < 0.7$. For heat release rate, the discussed trend is weakly (if any) pronounced, see figure 5(b).

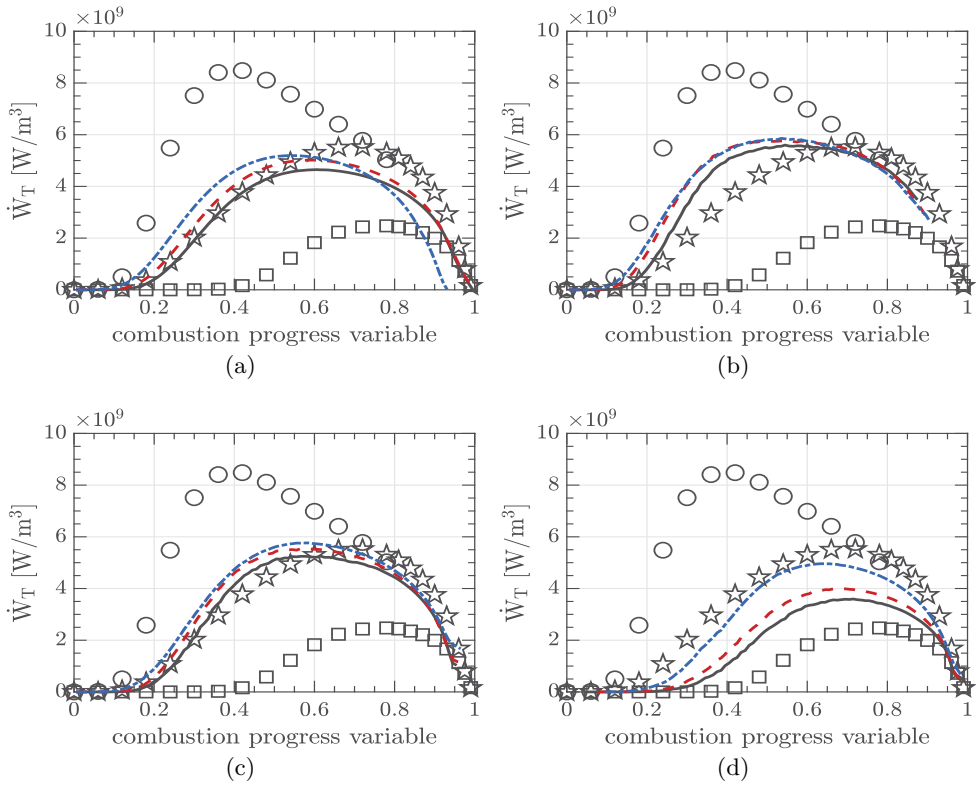

FIGURE 5. Time-averaged conditioned profiles of heat release rate. Legends are explained in caption to figure 2.

domain, whereas molecular transport plays an important role in the leading and trailing zones of the mean flame brush and significantly affects bulk turbulent burning velocity.

The results reported in figures 1-6 raise at least three questions:

- Why are differential diffusion effects more pronounced at the edges of the mean flame brush?
- Why is turbulent burning velocity more sensitive to differential diffusion effects localized to the leading edge?
- Why do trends observed for the conditioned profile of heat release rate, sampled from the leading edge, see figure 5(b), differ from trends observed for the conditioned profiles of fuel consumption rate, see figure 4(b)?

These three and one more questions are discussed in the next four subsections, with the focus of discussion being placed on a family of C-flames (C and C1, as well as C1/H and C1/H_2, which will be discussed later), because they are characterized by higher Karlovitz numbers when compared to four other flames (A1, A1, B, and B1).

3.2. *Why are differential diffusion effects more pronounced at the leading edge?*

The most evident explanation of a significant increase in the equivalence ratio, fuel consumption rate, or mass fraction of H at the leading edge of a mean flame brush consists in highlighting effects that stem from the local curvature of reaction zones. Indeed, first, from purely topological reasoning, local flame curvature should be predominantly positive at low $\langle c \rangle$ and predominantly negative at large $\langle c \rangle$. A decrease (increase) in the probability of finding positively (negatively) curved flames with $\langle c \rangle$ was documented in

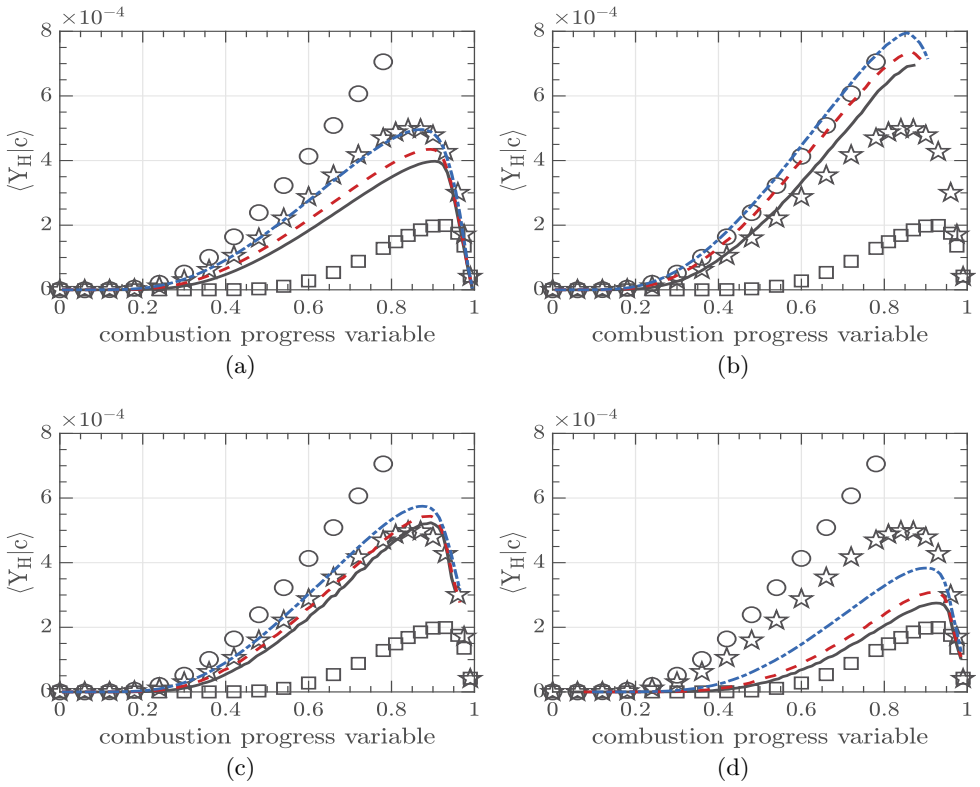

FIGURE 6. Time-averaged conditioned profiles of hydrogen mass fraction Y_H. Legends are explained in caption to figure 2.

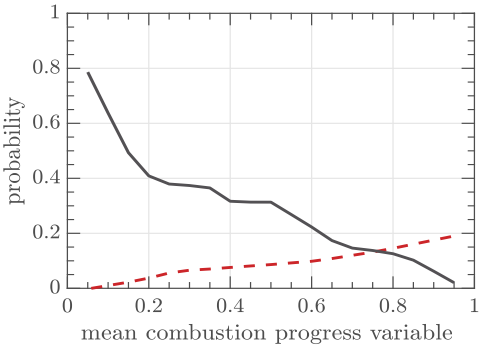

FIGURE 7. Probabilities of finding $\delta_L h_m > 1$ (black solid line) and $\delta_L h_m < -1$ (red dashed line) vs. transverse and time-averaged combustion progress variable $\bar{c}$. The probabilities have been sampled from flame zones characterized by a sufficiently high local fuel consumption rate (larger than 10 % of its peak value in the unperturbed laminar flame). Case C.

earlier DNS studies (Sabelnikov et al. 2021, figure 8a). This trend is also observed in figure 7, with the probability of finding highly curved reaction zones being large at low $\bar{c}$.

Second, theories of laminar premixed flames stretched by large-scale flow perturbations (Class et al. 2003; Kelley et al. 2012; Matalon & Matkowsky 1982; Pelcé & Clavin 1982; Zel'dovich et al. 1985) predict a significant influence of flame curvature on the local

burning rate and, in particular, an increase in the burning rate in positively curved flames if $Le < 1$. This increase stems from the local (i) enrichment (for lean hydrogen-air flames) and (ii) preheating of the reaction zone due to imbalances of (i) molecular fluxes of fuel and oxygen towards the reaction zone and (ii) molecular fluxes of the reactants towards the zone and molecular heat transfer from it.

For instance, the molecular diffusion term in the transport equation for a species mass fraction Y_k can be decomposed as follows (Peters 2000)

$$\underbrace{\nabla \cdot (\rho D_k \nabla Y_k)}_{T_0} = \underbrace{\boldsymbol{n}_k \cdot \nabla (\rho D_k \boldsymbol{n}_k \cdot \nabla Y_k)}_{T_1} \underbrace{-\rho D_k |\nabla Y_k| \nabla \cdot \boldsymbol{n}_k}_{T_2}, \tag{3.3}$$

where $\boldsymbol{n}_k = -\nabla Y_k / |\nabla Y_k|$ is the unit vector normal to an iso-surface of $Y_k(\boldsymbol{x}, t)$ =const. Term T_2 is directly proportional to curvature of the iso-surface and is known as curvature term. For major reactants (H_2 and O_2), this term is positive in a positively curved (i.e., $\nabla \cdot \boldsymbol{n} > 0$) reaction zone, because $\boldsymbol{n} \cdot \boldsymbol{n}_k < 0$ for these reactants. Recall that symbol $\boldsymbol{n}$ designates the unit vector normal to an iso-surface of $c(\boldsymbol{x}, t)$ =const, i.e., $\boldsymbol{n} = -\nabla c / |\nabla c|$. Moreover, the curvature term T_2 is larger for the fuel, because D_{H_2} is significantly larger than D_{O_2}. As a result, the mass fraction of H_2 and, hence, the local equivalence ratio is increased in positively curved reaction zones in the case of a lean hydrogen-air mixture. Since D_{H_2} is also significantly larger than the molecular heat diffusivity κ of such a mixture, similar arguments could be used to emphasize an increase in the local temperature in positively curved reaction zones. On the contrary, for atomic hydrogen, $T_2 > 0$ in negatively curved reaction zones, because $\boldsymbol{n} \cdot \boldsymbol{n}_H > 0$ in the largest part of a reaction zone, with the exception of a radical recombination region (Williams 2000) characterized by c close to unity.

An important role played by term T_2 is shown in figures 8 and 9, which report dependencies of doubly conditioned (on the local combustion progress variable c and curvature h_m) terms T_j on h_m and c, respectively. In particular, figure 8(a) shows that, for H_2, both the total diffusion term $\langle T_0 | c = 0.75 | h_m \rangle$ (black solid line) and the curvature term $\langle T_2 | c = 0.75 | h_m \rangle$ (blue dotted line) are significantly increased by curvature if $|\delta_l h_m| < 2$, whereas dependence of the normal diffusion term $\langle T_1 | c = 0.75 | h_m \rangle$ on h_m is less pronounced and non-monotonous, with T_1 peaking at a slightly negative curvature. Note that these results are conditioned to $c = 0.75 \pm 0.02$, because the highest (over the computational domain and time) fuel consumption rate is found at a close value of the combustion progress variable in flame C. For the radical H, the curvature term T_2 also plays an important role, but results in decreasing T_0 with h_m, as already noted when discussing (3.3).

The same trends are observed in figure 9, which shows dependencies of $\langle T_j | c | h_m \rangle$ on c, conditioned to $\delta_L h_m = -1 \pm 0.005$ (blue dotted lines), 0 ± 0.005 (red dashed lines), and 1 ± 0.005 (black solid lines). The curvature term T_2 results in increasing the molecular diffusion flux $\nabla \cdot (\rho D_k \nabla Y_k)$ (i) for H_2 if the local curvature is positive and (ii) for H if the local curvature is negative.

It is also of interest to note that time-averaged dependencies of $\langle T_j | c \rangle$ on c, sampled from the leading and trailing zones of the mean flame brush, look similar to dependencies of $\langle T_j | c | h_m \rangle$ on c, conditioned to $\delta_L h_m = 1 \pm 0.005$ and -1 ± 0.005, respectively, cf. curves plotted in black solid and blue dotted lines, respectively, in figures 9 and 10. This similarity (i) is associated with predominance of the positive and negative curvature at $\langle c \rangle = 0.1 \pm 0.02$ and 0.9 ± 0.02 respectively, see figure 7, and (ii) supports a hypothesis that differential diffusion effects are more pronounced at the leading and trailing edges

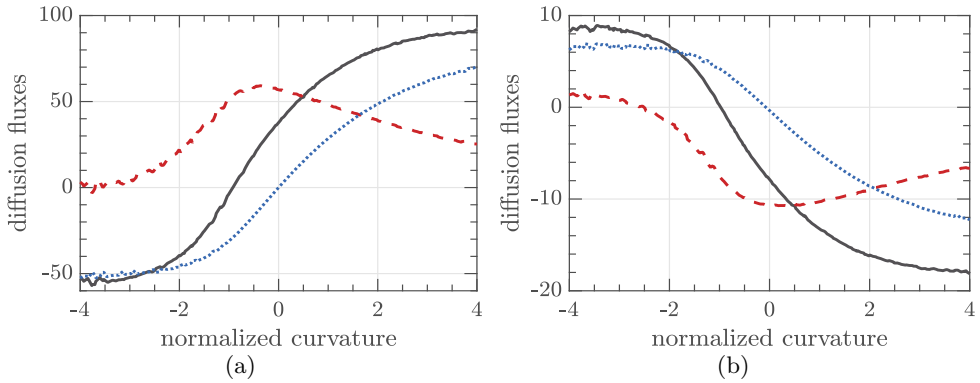

FIGURE 8. Time-averaged dependencies of molecular diffusion terms $\langle T_j|c|h_m\rangle$ on the normalized local curvature $\delta_L h_m$, sampled for (a) H_2 and (b) H at $c = 0.75 \pm 0.02$ from the entire flame brush in case C. Black solid, red dashed, and blue dotted lines show T_0, T_1, and T_2, respectively.

of the mean flame brush, because the local reaction zones are highly curved at small and large $\langle c\rangle$, with the curvature signs being opposite at these two values of $\langle c\rangle$.

Due to imbalance of molecular diffusion fluxes of H_2, O_2, and heat to and from curved reaction zones, the local temperature, equivalence ratio, fuel consumption rate, and mass fraction of H are increased by curvature, as reported in figure 11. However, these quantities are substantially affected not only by the curvature. For instance, dependencies of $\langle T|c = 0.75|h_m\rangle$, $\langle \phi|c = 0.75|h_m\rangle$, $\langle \dot{\omega}_{H_2}|c = 0.75|h_m\rangle$, and $\langle Y_H|c = 0.75|h_m\rangle$ on $\delta_L h_m$ sampled at $\langle c\rangle = 0.1 \pm 0.02$ and 0.9 ± 0.02 are substantially different, cf. black solid and blue dotted lines. Accordingly, dependencies of $\langle T|c|h_m\rangle(c)$, $\langle \phi|c|h_m\rangle(c)$, $\langle \dot{\omega}_{H_2}|c|h_m\rangle(c)$, and $\langle Y_H|c|h_m\rangle(c)$ on c, sampled from these two zones, are also substantially different, cf. left and right columns in figure 12. Effects of other flow characteristics on the conditioned quantities $\langle q|c\rangle$ and behaviour of the doubly conditioned heat release rate $\langle \dot{\omega}_T|c|h_m\rangle$ will further be addressed in sections 3.4 and 3.5, respectively.

3.3. *Leading point concept*

The DNS results plotted in figures 1 and 2-6 indicate that both turbulent burning velocities and the conditioned profiles of T, ϕ, $\dot{\omega}_{H_2}$, $\dot{\omega}_T$, and Y_H, sampled at $\langle c\rangle = 0.1 \pm 0.02$ are significantly affected by Le, whereas the conditioned profiles of the same quantities, sampled from the middle of the C-flame brush, are associated with $Le = 1$. This observation not only shows that differences in molecular transport coefficients of reactants and/or heat play a more important role at the leading edge of a mean turbulent flame brush, but also implies that the turbulent burning velocities are controlled by processes localized to the leading edge. This implication is in line with (i) the so-called KPP theory of convection-diffusion-reaction waves developed by Kolmogorov et al. (1937) and extended in subsequent studies reviewed elsewhere (Ebert & van Saarlos 2000; Sabelnikov et al. 2016) and (ii) Zel'dovich's idea about the crucial role played by leading points in propagation of premixed turbulent flames. That idea was developed in USSR several decades ago, as reviewed elsewhere (Kuznetsov & Sabelnikov 1990; Lipatnikov & Chomiak 2005), and was supported in recent theoretical (Kha et al. 2016; Sabelnikov & Lipatnikov 2013, 2015), experimental (Venkateswaran et al. 2011, 2013, 2015; Zhang et al. 2018), and DNS (Amato et al. 2015a,b; Dave et al. 2018; Kim 2017; Lipatnikov et al. 2018) studies, as well as in earlier single-step chemistry (Karpov et al. 1996) or recent complex chemistry (Verma et al. 2021) Reynolds-Averaged Navier Stokes (RANS) simulations of experi-

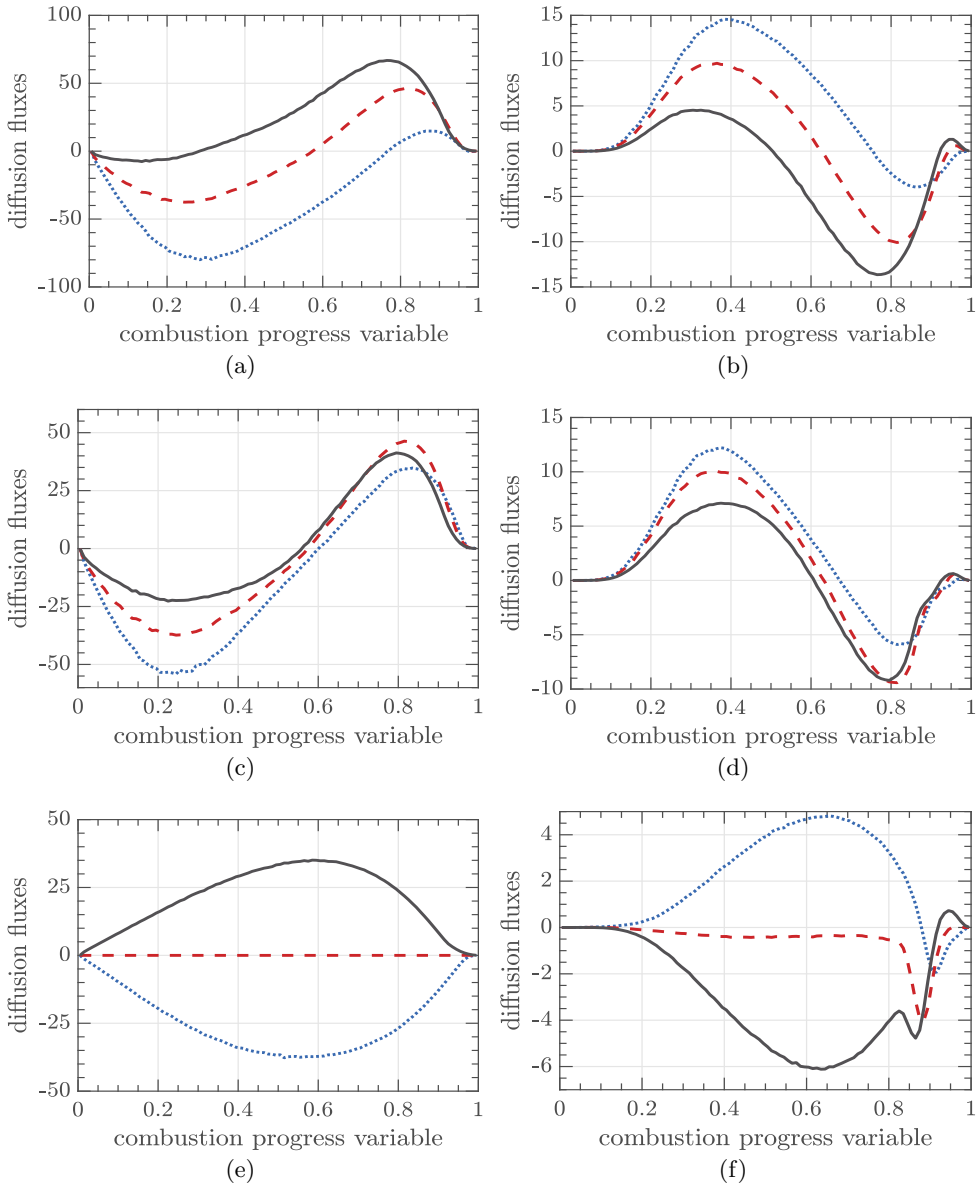

FIGURE 9. Time-averaged dependencies of molecular diffusion terms on the local combustion progress variable c, sampled at $\delta_L h_m = -1 \pm 0.005$ (blue dotted lines), 0 ± 0.005 (red dashed lines), and 1 ± 0.005 (black solid lines) from the entire flame brush in case C. (a) $\langle T_0|c|h_m\rangle$ for H_2, (b) $\langle T_0|c|h_m\rangle$ for H, (c) $\langle T_1|c|h_m\rangle$ for H_2, (d) $\langle T_1|c|h_m\rangle$ for H, (e) $\langle T_2|c|h_m\rangle$ for H_2, and (f) $\langle T_2|c|h_m\rangle$ for H.

ments with lean H_2/air (Karpov & Severin 1980) or H_2/CO/air (Venkateswaran et al. 2011, 2013) flames, respectively.

The present work further supports the leading point concept by showing its consistency with recent DNS data that indicate mitigation of the influence of Le on the conditioned profiles of local flame characteristics in intense turbulence. And vice versa, the leading

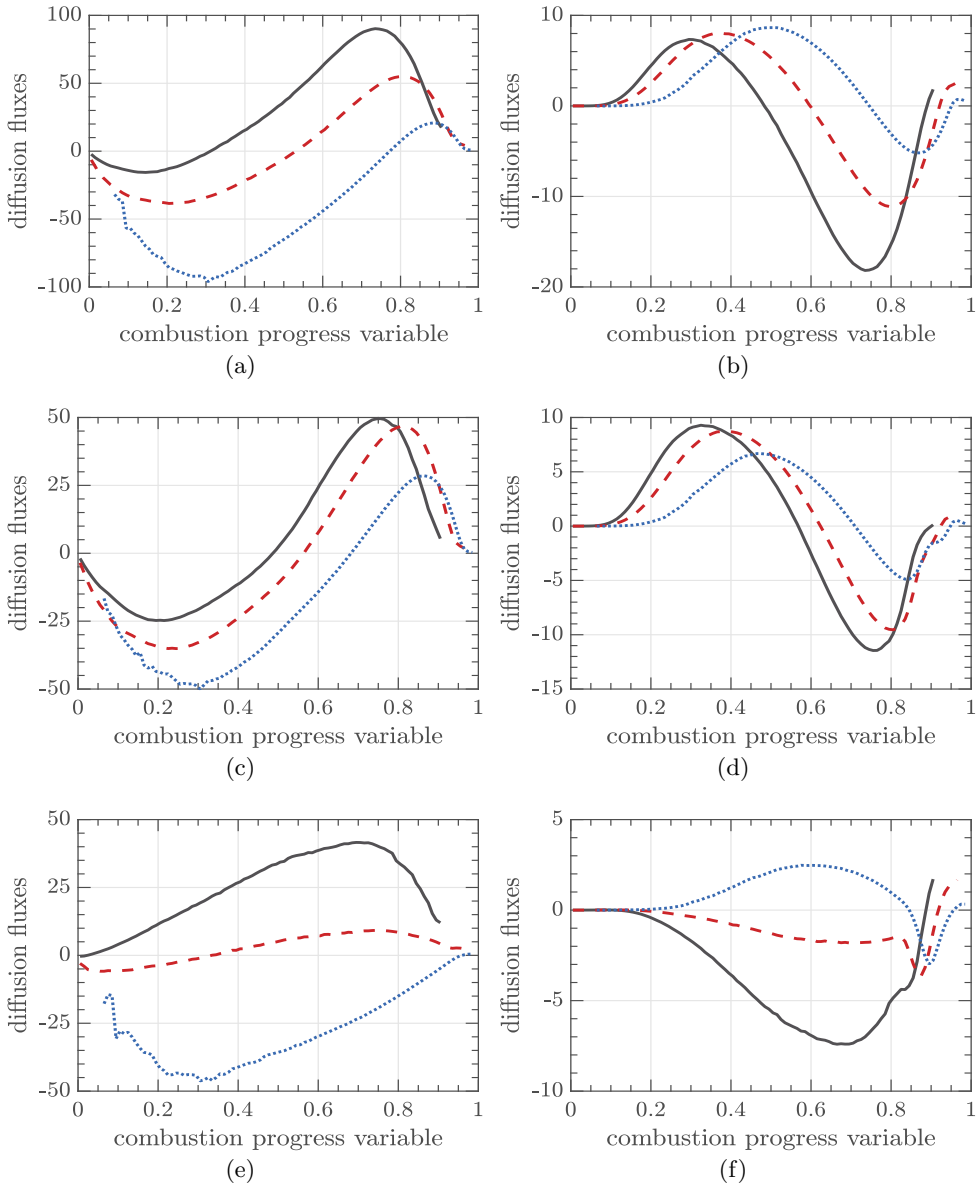

FIGURE 10. Time-averaged dependencies of conditioned molecular diffusion terms on the local combustion progress variable, sampled at $\langle c \rangle = 0.1 \pm 0.02$ (black solid lines), 0.5 ± 0.02 (red dashed lines), and 0.9 ± 0.02 (blue dotted lines) in flame C. (*a*) $\langle T_0|c \rangle$ for H_2, (*b*) $\langle T_0|c \rangle$ for H, (*c*) $\langle T_1|c \rangle$ for H_2, (*d*) $\langle T_1|c \rangle$ for H, (*e*) $\langle T_2|c \rangle$ for H_2, and (*f*) $\langle T_2|c \rangle$ for H.

point concept supports consistency of the two investigated findings by hypothesizing that U_t is controlled by processes localized to the leading edge of the mean flame brush.

Moreover, complex-chemistry DNS of lean hydrogen-air turbulent flames offer the following opportunity for probing the leading point concept. Among nine species included into the state-of-the-art chemical mechanisms of hydrogen combustion and in the mechanism by Kéromnès et al. (2013) used in the present study, only atomic hydrogen H and molecular hydrogen H_2 are characterized by molecular diffusivities much larger than the

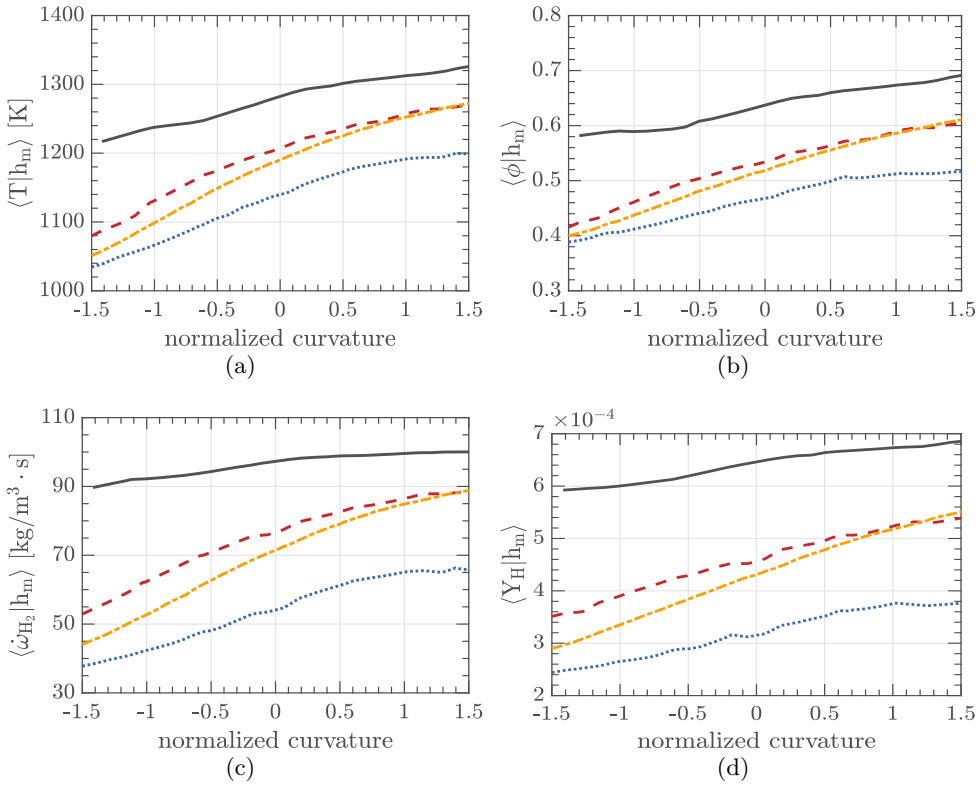

FIGURE 11. Time-averaged dependencies of doubly conditioned (a) temperature $\langle T|c = 0.75|h_m\rangle$, ($b$) equivalence ratio $\langle\phi|c = 0.75|h_m\rangle$, ($c$) fuel consumption rate $\langle\dot{\omega}_{H_2}|c = 0.75|h_m\rangle$, and ($d$) hydrogen mass fraction $\langle Y_H|c = 0.75|h_m\rangle$ on the normalized local curvature $\delta_L h_m$, sampled from the entire flame brush (orange dotted-dashed lines), its leading zone characterized by $\langle c\rangle(y,t) = 0.1 \pm 0.02$ (black solid lines), middle zone ($\langle c\rangle = 0.5 \pm 0.02$, red dashed lines), and trailing zone ($\langle c\rangle = 0.9 \pm 0.02$, blue dotted lines). Case C.

diffusivity of O_2 or heat diffusivity of the mixture. At the same time, as discussed earlier, molecular diffusion of H_2 results in increasing (when compared to the unperturbed laminar flame) equivalence ratio in positively curved reaction zones, whereas molecular diffusion of H from recombination to reaction zones results in increasing Y_H in negatively curved reaction zones. Accordingly, one may assume that an increase in local burning rate should predominantly be observed (i) in negatively curved reaction zones concentrating in the trailing edge of a mean flame brush if Lewis numbers are equal to unity for all species with the exception of H, but (ii) in positively curved reaction zones concentrating in the leading edge of a mean flame brush if Lewis numbers are equal to unity for all species with the exception of H_2.

Based on the above reasoning, two extra DNS cases C1/H and C1/H2 were run by using the mixture-averaged molecular diffusivities of H and H_2, respectively, and setting Lewis numbers equal to unity for all other species. The computed results sampled from the entire flame brushes do show that the equivalence ratio, fuel consumption rate, heat release rate, and mass fraction of H conditioned to positive curvature are larger than their values conditioned to negative curvature in case C1/H2, cf. blue solid and dashed

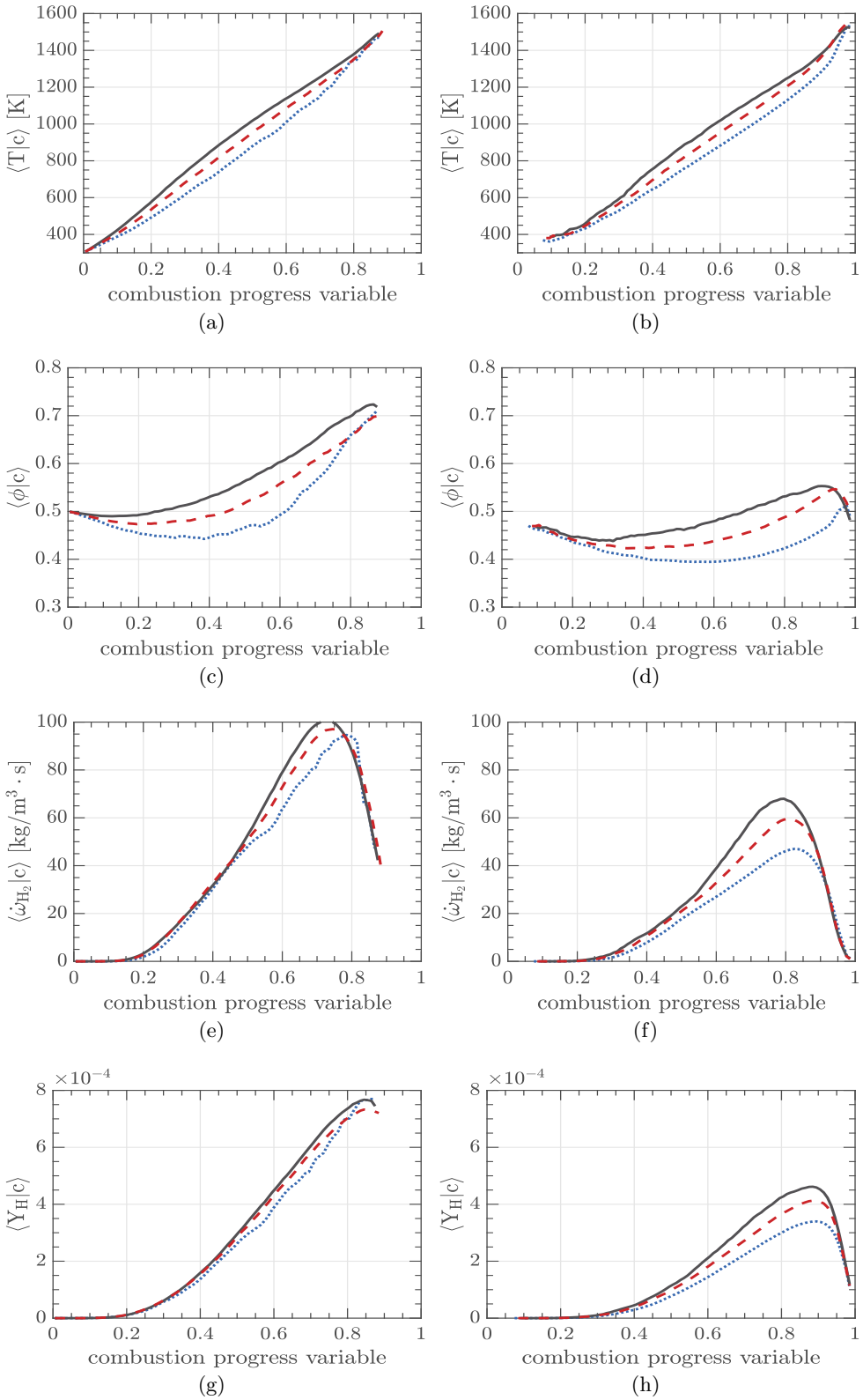

FIGURE 12. Time-averaged dependencies of doubly conditioned (*a*) and (*b*) temperature $\langle T|c|h_m\rangle$, (*c*) and (*d*) equivalence ratio $\langle\phi|c|h_m\rangle$, (*e*) and (*f*) fuel consumption rate $\langle\dot{\omega}_{H_2}|c|h_m\rangle$, and (*g*) and (*h*) hydrogen mass fraction $\langle Y_H|c=|h_m\rangle$ on c, obtained at $\delta_L h_m = -0.1 \pm 0.005$ (blue dotted lines), 0 ± 0.005 (red dashed lines), and 1 ± 0.005 (black solid lines) in case C. Results sampled from the leading and trailing zones of the flame brush are reported in cells (*a*), (*c*), (*e*), (*g*) and (*b*), (*d*), (*f*), (*h*), respectively.

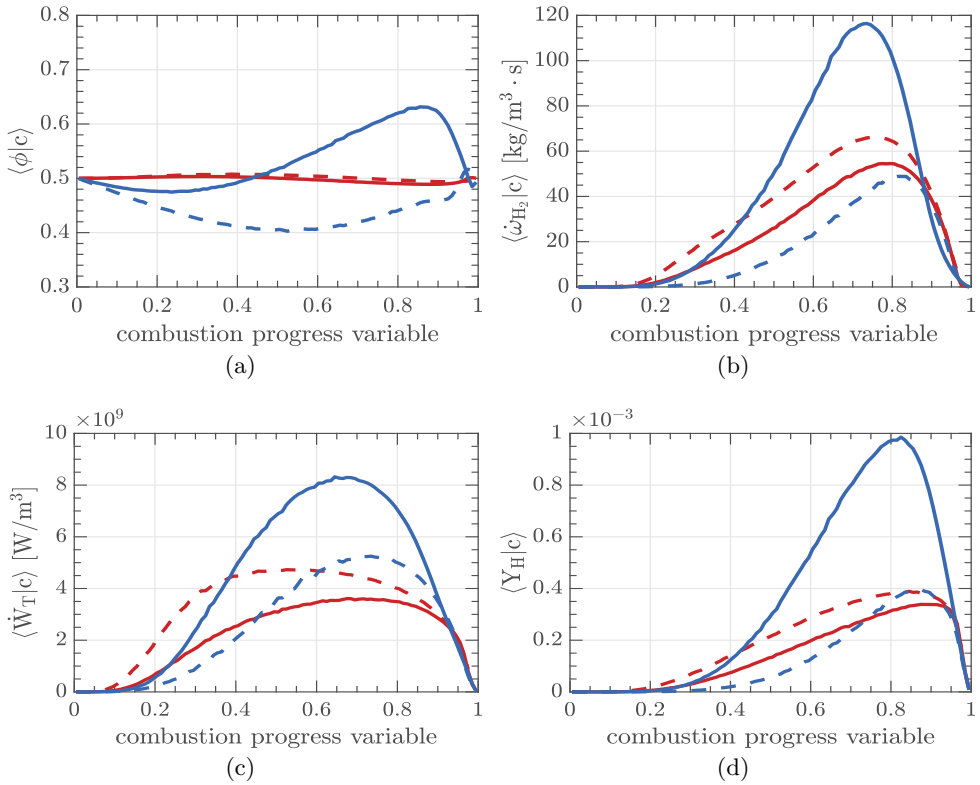

FIGURE 13. Time-averaged dependencies of doubly conditioned (a) equivalence ratio $\langle\phi|c|h_m\rangle$, (b) fuel consumption rate $\langle\dot{\omega}_{H_2}|c|h_m\rangle$, ($c$) heat release rate $\langle\dot{\omega}_T|c|h_m\rangle$, and ($d$) hydrogen mass fraction $\langle Y_H|c|h_m\rangle$ on combustion progress variable. Results conditioned to $\delta_L h_m = -1 \pm 0.005$ and $\delta_L h_m = 1 \pm 0.005$ are shown in dashed and solid lines, respectively. Results obtained from flames C1/H and C1/H2 are plotted in red and blue lines, respectively.

lines in figure 13, whereas the opposite trend is observed in case C1/H, cf. red solid and dashed lines.

Significant influence of molecular diffusion of atomic hydrogen on local burning structures was recently explored by Rieth et al. (2021) by analyzing DNS data obtained from (i) preheated lean $NH_3/H_2/N_2$-air flames propagating in a turbulent shear layer and (ii) statistically planar highly preheated lean hydrogen-air turbulent flames. In particular, by turning-off molecular diffusivity of H, Rieth et al. (2021) have shown that enhanced molecular transport of atomic hydrogen into negatively curved low-temperature heat release zones results in significantly increasing local heat release rate. A similar effect is observed in figure 13(c).

The qualitative difference between the present cases C1/H and C1/H2 is also demonstrated in figure 14, where doubly conditioned profiles of $\langle\dot{\omega}_{H_2}|c|h_m\rangle(c)$, $\langle\dot{\omega}_T|c|h_m\rangle(c)$, and $\langle Y_H|c|h_m\rangle(c)$ sampled from the leading (red or blue lines) and trailing (black lines) zones are reported. Moreover, figures 14(b), 14(d), and 14(f) show that fuel consumption rate, heat release rate, and mass fraction of H, respectively, conditioned to $\langle c\rangle = 0.1 \pm 0.02$ are larger than their values conditioned to $\langle c\rangle = 0.9 \pm 0.02$ in flame C1/H2, cf. blue and black curves, respectively. In flame C1/H, the opposite trend is documented, cf. red and black curves in figures 14(a), 14(c), or 14(e).

In addition to figures 13 and 14, which present doubly conditioned c-profiles for two in-

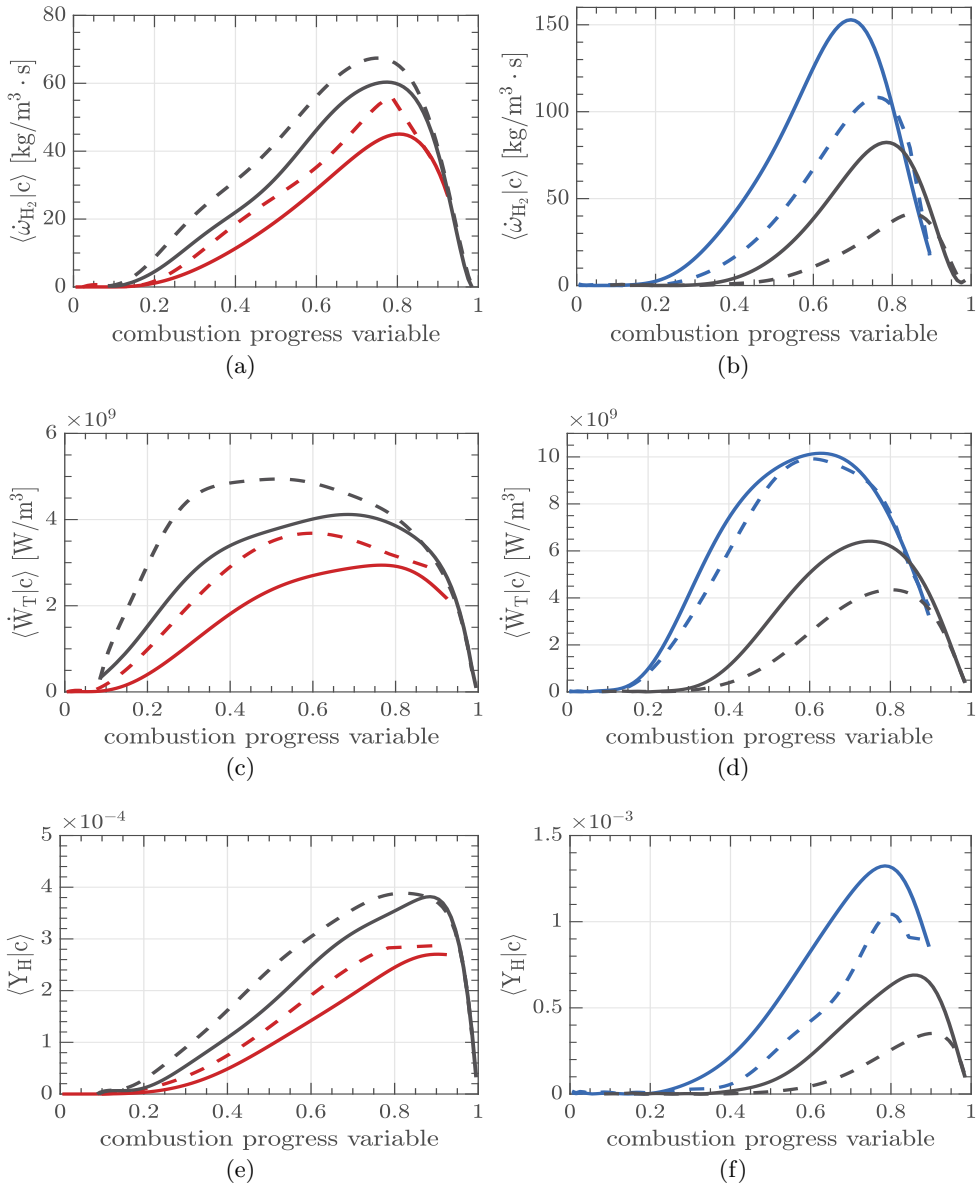

FIGURE 14. Time-averaged dependencies of doubly conditioned (a) and (b) fuel consumption rate $\langle \dot{\omega}_{H_2}|c|h_m\rangle$, ($c$) and ($d$) heat release rate $\langle \dot{\omega}_T|c|h_m\rangle$, and ($e$) and ($f$) hydrogen mass fraction $\langle Y_H|c|h_m\rangle$ on combustion progress variable, sampled at $\langle c\rangle = 0.1 \pm 0.02$ (red or blue lines) and 0.9 ± 0.02 (black lines) Results conditioned to the negative $\delta_L h_m = -1 \pm 0.005$ or positive $\delta_L h_m = 1 \pm 0.005$ are shown in dashed or solid lines, respectively. (a), (c), and (e) - case C1/H; (b), (d), and (f) - case C1/H2.

tervals of curvature (negative and positive), figure 15 reports simply conditioned profiles of $\langle \dot{\omega}_{H_2}|c\rangle(c)$, $\langle \dot{\omega}_T|c\rangle(c)$, and $\langle Y_H|c\rangle(c)$ sampled from the leading (left column) and trailing (right column) zones of mean flame brushes in four C-cases. Comparison of results plotted in blue dotted and orange dotted-dashed lines show that preferential diffusion of molecular hydrogen results in increasing (decreasing) fuel consumption rate, heat re-

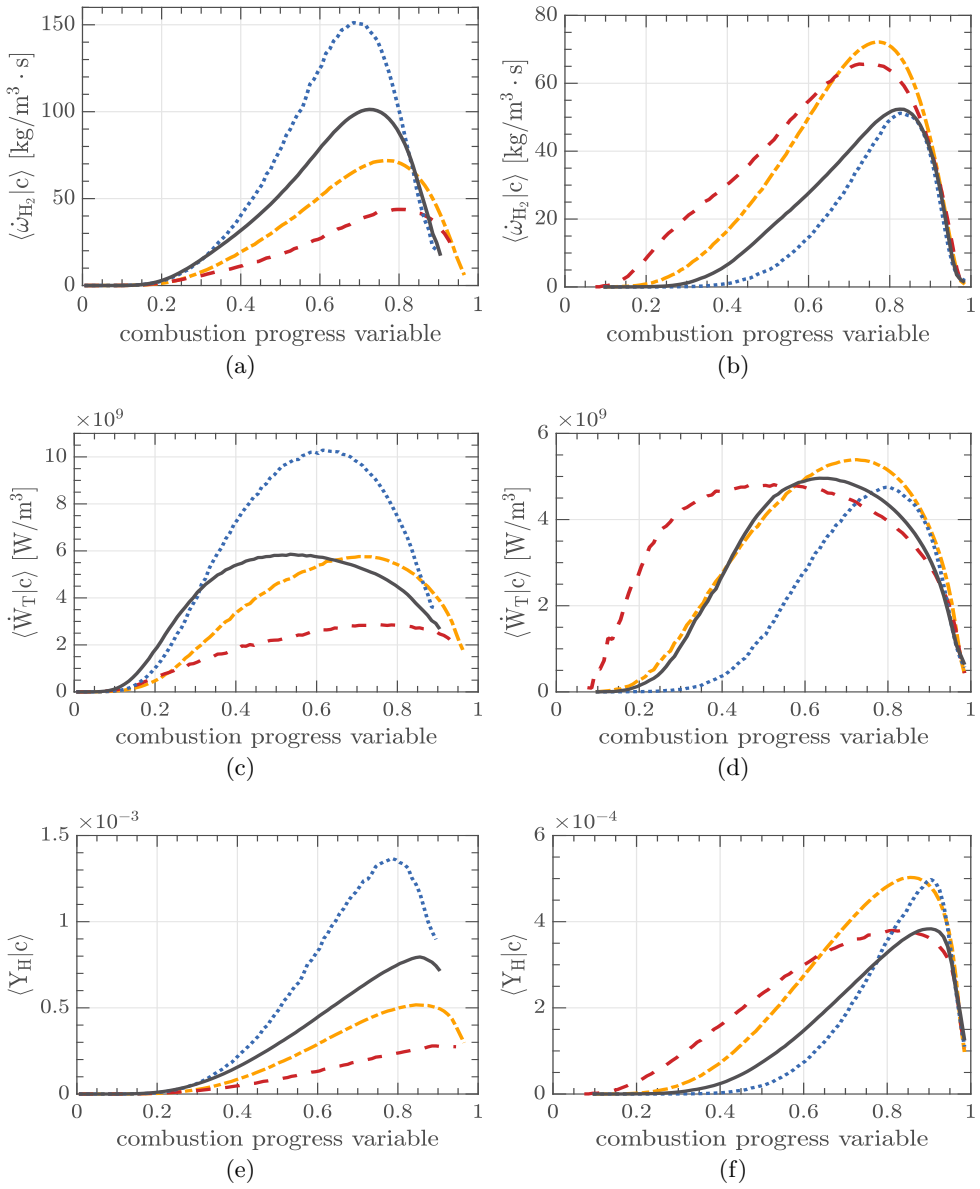

FIGURE 15. Time-averaged dependencies of conditioned (a) and (b) fuel consumption rate $\langle\dot{\omega}_{H_2}|c\rangle$, (c) and (d) heat release rate $\langle\dot{\omega}_T|c\rangle$, and (e) and (f) hydrogen mass fraction $\langle Y_H|c\rangle$ on combustion progress variable, sampled (a), (c), and (e) at $\langle c\rangle = 0.1 \pm 0.02$ or (b), (d), and (f) at 0.9 ± 0.02 Results obtained in case C, C1, C1/H, and C1/H2 are plotted in black solid, orange dotted-dashed, red dashed, and blue dotted lines, respectively.

lease rate, and mass fraction of H at $\langle c\rangle = 0.1 \pm 0.02$ (0.9 ± 0.02, respectively), with differential diffusion of other species acting in the opposite direction, cf. blue dotted and black solid lines. Comparison of results plotted in red dashed and orange dotted-dashed lines show that preferential diffusion of atomic hydrogen results in increasing (decreasing) $\langle\dot{\omega}_{H_2}|c\rangle(c)$, $\langle\dot{\omega}_T|c\rangle(c)$, and $\langle Y_H|c|h_m\rangle(c)$ at $c < 0.6$ and $\langle c\rangle = 0.9 \pm 0.02$ (various c and $\langle c\rangle = 0.1 \pm 0.02$, respectively).

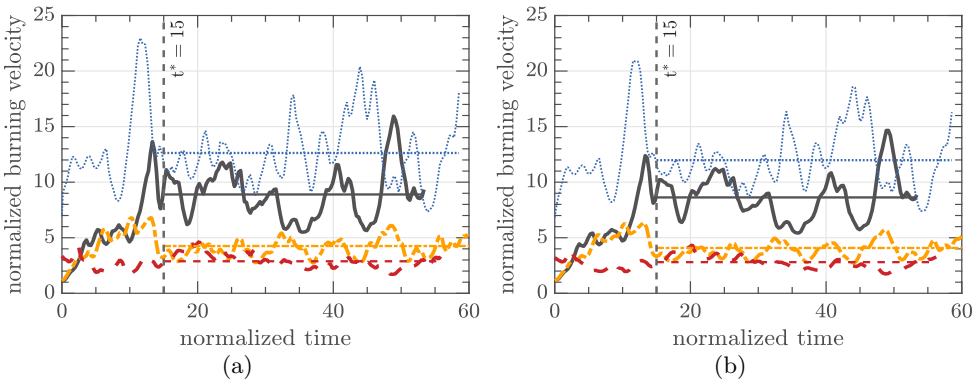

FIGURE 16. Evolution of the normalized turbulent burning velocities (*a*) U_t^F/S_L and (*b*) U_t^T/S_L in flames C (black solid lines), C1 (orange dotted-dashed lines), C1/H (red dashed lines), and C1/H2 (blue dotted lines). Horizontal straight lines show mean values.

Thus, figures 13-15 imply that differential diffusion effects accelerate burning at the leading edge of the C1/H2 flame brush or at the trailing edge of the C1/H flame brush (if $c < 0.6$). Therefore, turbulent burning velocities computed in the two cases offer an opportunity to compare contributions of the leading and trailing edges to the bulk combustion rate. Figure 16 shows that, among four C-cases, the highest and lowest turbulent burning velocities are obtained in cases C1/H2 (blue dotted lines) and C1/H (red dashed lines), respectively. This result highlights the leading edge. Moreover, comparison of blue dotted and black solid lines indicates that differential diffusion effects for all species with the exception of H_2 reduce turbulent burning velocity. In particular, differential diffusion effects for H do so, cf. red dashed and orange dotted-dashed lines. The decrease in the turbulent burning velocity in case C1/H when compared to case C1 is associated with lower fuel consumption and heat release rates at $\langle c \rangle = 0.1 \pm 0.02$, cf. curves plotted in red dashed and orange dotted-dashed lines, respectively, in figures 15(a) and 15(c). While these rates are higher in case C1/H at $\langle c \rangle = 0.9 \pm 0.02$, see figures 15(b) and 15(d), the turbulent burning velocities show the opposite trend, thus, indicating the special role played by the leading edge.

It is worth remembering, however, that the KPP theory was developed for a specific set of source terms in the convection-diffusion-reaction equation (Kolmogorov et al. 1937). For another set of source terms, wave propagation can be controlled by processes localized to its trailing edge. A laminar premixed flame described by the classical Zel'dovich-Frank-Kamenetskii theory (Zel'dovich & Frank-Kamenetskii 1938; Zel'dovich et al. 1985) is an example of such a pushed wave (van Saarloos 2003). Transition from pulled flames whose speed is controlled by processes localized to its leading edge to pushed flames was earlier explored by Aldushin et al. (1979), Zel'dovich (1980), Clavin & Liñán (1984), Sabelnikov & Lipatnikov (2015), and Sabelnikov et al. (2016). Such a transition can also occur in turbulent flows. For instance, differential diffusion of atomic hydrogen into negatively curved cusps close to the trailing zone of a turbulent flame brush could promote local auto-ignition, which substantially accelerates flame propagation. However, such an effect has yet been found in highly preheated mixtures only (Gruber et al. 2021; Rieth et al. 2021). At the room temperature and, in particular, under conditions of the present study, turbulent flames appear to be pulled waves.

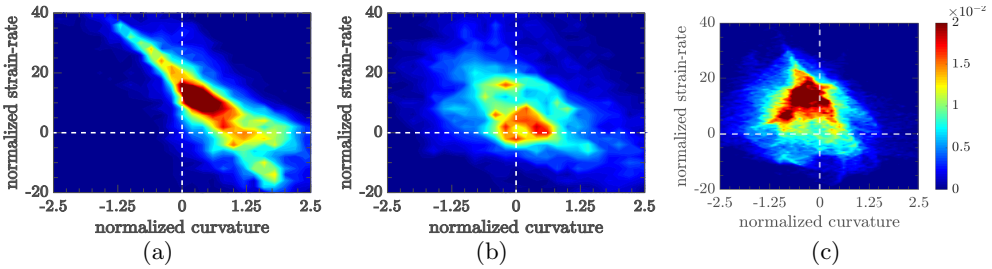

FIGURE 17. Joint Probability Density Functions for normalized curvature $\delta_L h_m$ and normalized strain rate $\tau_f a_t$ sampled at (a) $\langle c \rangle = 0.1 \pm 0.02$, (b) $\langle c \rangle = 0.5 \pm 0.02$, and (c) $\langle c \rangle = 0.9 \pm 0.02$. Case C.

3.4. *Turbulent combustion and perturbed laminar flames*

Within the framework of the leading point concept, an increase in turbulent burning velocity with decreasing Lewis number in lean hydrogen-air turbulent flames is proposed to be modeled by substituting characteristics of the unperturbed laminar flame with characteristics of a highly perturbed laminar flame (Kuznetsov & Sabelnikov 1990; Lipatnikov & Chomiak 2005). Accordingly, selection of a laminar flame configuration that is most appropriate for modeling the local structure of the leading points in a turbulent flow (Lipatnikov & Chomiak 1998) is of significant fundamental and applied interest. While this issue is beyond the major scope of the present paper, a few comments follow.

First, certain results discussed earlier highlight local flame curvature, but also show that the list of important local flame perturbation characteristics is not limited to the curvature, e.g. see figure 11, where dependencies of various quantities on curvature are different for different zones of the mean flame brush. Such a list should involve other local flame or flow characteristics, e.g., strain rate. Indeed, since the pioneering study by Klimov (1963), local strain rate is well known to significantly affect flame structure and burning rate, with such effects are expected to be of great importance in highly turbulent flows (Abdel-Gayed et al. 1984b; Bradley et al. 2005; Bray & Cant 1991; Lipatnikov & Chomiak 2005), where the normalized strain rates $\tau_f a_t$ can be large.

Figure 17 shows that joint Probability Density Function (PDF) for normalized curvature $\delta_L h_m$ and normalized strain rate $\tau_f a_t$ varies substantially with $\langle c \rangle$. Accordingly, differences between four curves in figure 11 could be attributed to strain-rate effects, which should be different in the leading, middle, and trailing zones of the mean flame brush due to significant differences between the PDFs plotted in figures 17(a), 17(b), and 17(c), respectively. Such an explanation could also be interpreted as an indication that strain rate is one more important characteristic of the local structure of the leading points, in line with the theories of perturbed laminar flames (Class et al. 2003; Kelley et al. 2012; Matalon & Matkowsky 1982; Pelcé & Clavin 1982; Zel'dovich et al. 1985).

However, second, it is worth remembering that the aforementioned theories address large-scale (when compared to the laminar flame thickness) perturbations. Under such conditions, a perturbation is quantified using a single value of curvature, a single value of strain rate, etc., i.e., the perturbation characteristics are considered to be the same in different flame zones. In a highly turbulent flame characterized by $Ka \gg 1$, the Kolmogorov length scale is much smaller than the local flame thickness and, consequently, the local flow characteristics such as strain rate vary significantly within the flame. To demonstrate such variations, points and instants characterized by the smallest values of $|n_x| \ll 1$ and $|n_z| \ll 1$ in the local reaction zones were selected in order for the

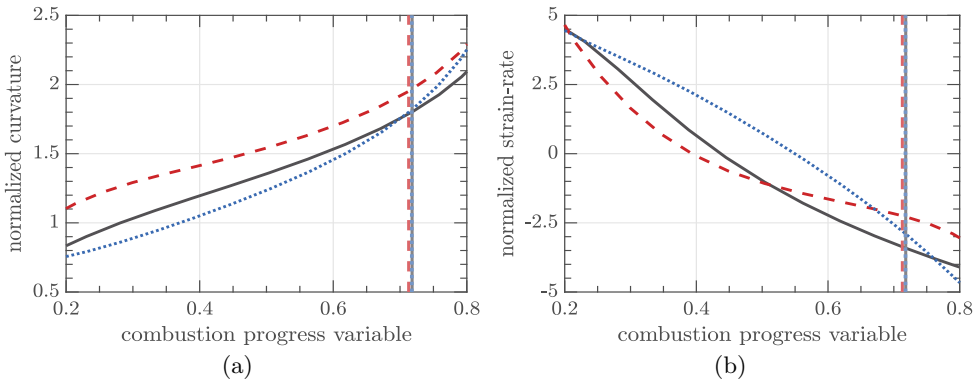

FIGURE 18. Instantaneous axial profiles of (a) normalized curvature $\delta_L h_m(y)$ and (b) normalized strain rate $\tau_f a_t(y)$, obtained at $t/\tau_t = 27.51$ (black solid lines), 65.67 (red dashed lines), and 70.20 (blue dotted lines) and presented vs. $c(y)$. Vertical straight lines show positions of the peak fuel consumption rate. Case B.

local profiles of $\delta_L h_m(y)$ or $\tau_f a_t(y)$ to show variations of the curvature and strain rate, respectively, along the normal to the reaction zone.

Such profiles obtained in case B at three instants are plotted in figure 18. While both curvature and strain rate vary with $c(y)$, variations in $\tau_f a_t$ are much more pronounced, with even sign of the local strain rate changing in the reaction zone. Accordingly, it is not clear what value of $\tau_f a_t$ should be used (i) to characterize turbulence-induced perturbations of the local flame structure or (ii) to calculate local combustion characteristics conditioned to strain rate.

Since the locally maximal fuel consumption or heat release rate is controlled by the local mixture composition and temperature, which, in their turn, are affected by molecular transport in upstream flame zones, strain rates evaluated at certain distance upstream of leading points are likely to be more appropriate for characterizing perturbations in the leading points at $Ka \gg 1$. Probably for these reasons, doubly conditioned profiles of $\langle q|a_t|c\rangle$ obtained by evaluating q, a_t, and c in the same point (not shown) do not reveal any clear trend regarding the influence of the strain rate on $\langle q|a_t|c\rangle$ in case C. This issue definitely requires further research and will be a subject for future study.

Moreover, it is also worth stressing that the influence of intense small-scale turbulence ($Ka \gg 1$) on a premixed flame is a highly unsteady phenomenon, because the life time of the smallest eddies is much shorter than the laminar flame time scale under such conditions. Therefore, a simple laminar flame configuration (stationary counter-flow flames, expanding spherical or cylindrical flame, a single cusp, etc.) is unlikely to allow researchers to model all major characteristics (temperature, equivalence ratio, fuel consumption and heat release rates, radical concentrations, etc.) of leading points in a highly turbulent flame.

Nevertheless, third, the fact that the profiles of $\langle\dot\omega_{H_2}|c\rangle(c)$ sampled at $\langle c\rangle = 0.1 \pm 0.02$ from flames A, B, and C are close to the profile of $\dot\omega_{H_2}(c)$ obtained from a highly strained planar stationary laminar flame, cf. lines with circles in figure 4(b), should not be ignored. This result does not mean that the highly strained planar stationary laminar flame is an appropriate model of the local structure of leading points in turbulent flames, e.g., the laminar-flame profiles of $\phi(c)$ and, especially, $\dot\omega_T(c)$ differ from $\langle\phi|c\rangle(c)$ and $\langle\dot\omega_T|c\rangle(c)$, respectively, cf. circles with lines in figures 3(b) and 5(b), respectively. However, the peak fuel consumption rate computed in a highly strained planar stationary laminar

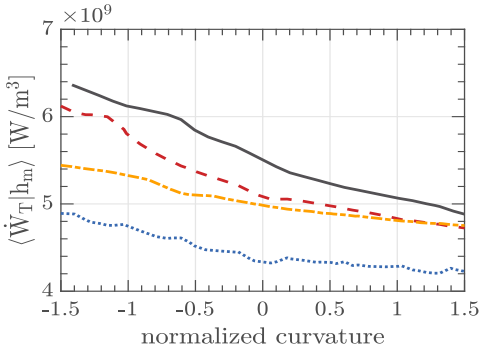

FIGURE 19. Time-averaged dependencies of doubly conditioned heat release rate $\langle \dot{\omega}_T | c = 0.75 | h_m \rangle$ on the normalized local curvature $\delta_L h_m$, sampled from the entire flame brush (orange dotted-dashed lines), its leading zone characterized by $\langle c \rangle(y,t) = 0.1 \pm 0.02$ (black solid lines), middle zone ($\langle c \rangle = 0.5 \pm 0.02$, red dashed lines), and trailing zone ($\langle c \rangle = 0.9 \pm 0.02$, blue dotted lines). Case C.

flame could still be useful for modeling turbulent burning velocity, as hypothesized by (Kuznetsov & Sabelnikov 1990) and confirmed in recent RANS simulations (Verma et al. 2021) of experiments with lean H_2/CO/air flames (Venkateswaran et al. 2011, 2013).

For instance, a recent analysis (Lee et al. 2021a,b) of extreme points, i.e., points characterized by the highest instantaneous fuel consumption or heat release rate over the entire computational domain, has shown that the extreme $\dot{\omega}_{H_2}(t)$ fluctuates weakly with time around a mean value, which is almost the same for the three flames A, B, and C characterized by significantly different Karlovitz numbers, see table 1. On the contrary, fluctuations of $\dot{\omega}_T(t)$ are more pronounced, with its mean value being substantially increased by Ka. These and other results discussed by Lee et al. (2021a,b) suggest that there is a maximal possible (for a specific mixture of unburned reactants under specific temperature and pressure) increase in the peak fuel consumption rate, with this extreme increase occurring in various highly perturbed reaction zones, including critically strained ones. This hypothesis requires further research and will be a subject for future study.

3.5. *Fuel consumption and heat release rates*

As noted in the end of the previous subsection, there are substantial differences in the behaviour of fuel consumption and heat release rates in highly perturbed reactions zones. Similar differences can be observed by comparing figures 4 and 5 or figures 11(c) and 19. These differences are associated with a phenomenon of decorrelation between local fuel consumption and heat release rate at low temperatures, explored by Carlsson et al. (2014), Aspden et al. (2015), Dasgupta et al. (2017) and also observed by analyzing the present DNS data obtained from flames A, B, and C (Lee et al. 2021a). For instance, curves plotted in figures 4 and 5 show that $\langle \dot{\omega}_{H_2} | c \rangle(c)$ and $\langle \dot{\omega}_T | c \rangle(c)$ peak at significantly different c (the latter rate peaks at a lower c) in the turbulent flames A, B, and C, whereas fuel consumption and heat release rates peak at sufficiently close c in the unperturbed laminar flame, see squares.

The decorrelation stems from the fact that three reactions that control heat release rate at low temperatures in lean hydrogen-air flames, i.e. $H+O_2+M \rightleftharpoons HO_2+M$, $HO_2+H \rightleftharpoons 2OH$, and $HO_2+OH \rightleftharpoons H_2O+O_2$ do not involve H_2, with the rates of these reactions being significantly increased in negatively curved reaction zones due to preferential diffusion of atomic hydrogen into them (Aspden et al. 2015).

Such effects manifest themselves in several figures. First, a decrease in $\langle \dot{\omega}_T | c = 0.75 | h_m \rangle$

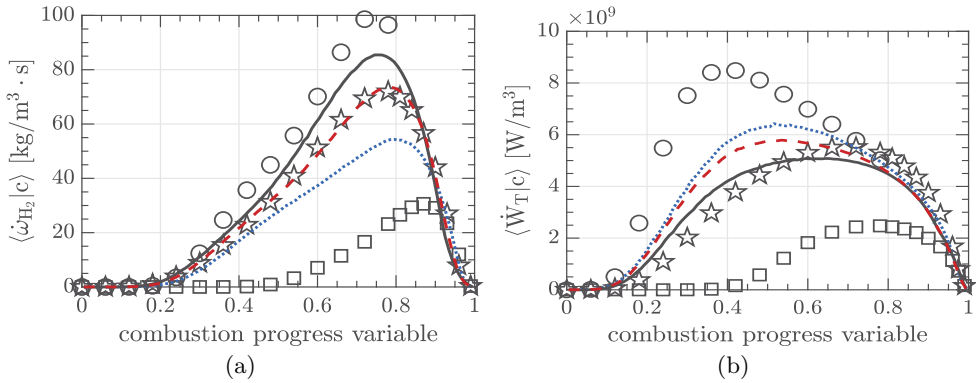

FIGURE 20. Time-averaged dependencies of doubly conditioned (a) fuel consumption rate $\langle\dot{\omega}_{H_2}|c|h_m\rangle$ and (b) heat release $\langle\dot{\omega}_T|c|h_m\rangle$ on c, obtained at $\delta_L h_m = -0.1 \pm 0.005$ (blue dotted lines), 0 ± 0.005 (red dashed lines), and 1 ± 0.005 (black solid lines) in case C. Symbols are explained in caption to figure 2.

with increasing curvature is observed in figure 19. Second, results plotted in red lines in figure 13(c) also show that heat release rate is significantly higher in negatively curved reaction zones, with the effect being most pronounced at $c < 0.4$. Third, the same trend is observed in figure 14(c), where results obtained from flame C1/H are reported. Fourth, due to preferential diffusion of atomic hydrogen into negatively curved reaction zones, the rate $\langle\dot{\omega}_{H_2}|c\rangle(c)$ sampled at $\langle c\rangle = 0.9 \pm 0.02$ from flame C1/H is larger (at $c \leqslant 0.6$) than $\langle\dot{\omega}_{H_2}|c\rangle(c)$ sampled at $\langle c\rangle = 0.9 \pm 0.02$ from flame C1, cf. red dashed and orange dotted-dashed lines, respectively, in figure 15(d). For these rates sampled at $\langle c\rangle = 0.1 \pm 0.02$, the opposite trend is observed in figure 15(c), because the probability of finding negatively curved reaction zones is low at low $\langle c\rangle$. Fifth, figures 20(a) and 20(b) show that $\langle\dot{\omega}_{H_2}|c|h_m\rangle$ is higher for positive curvatures, whereas $\langle\dot{\omega}_T|c|h_m\rangle$ is higher for negative curvatures, respectively.

The noted substantial differences in the behaviors of fuel consumption and heat release rates in turbulent flames imply that the basic idea of the leading point concept, i.e., the use of characteristics of highly perturbed laminar flames for evaluation of turbulent burning velocity (Kuznetsov & Sabelnikov 1990; Lipatnikov 2012), (i) is appropriate for the former rate $\dot{\omega}_{H_2}$, which is increased in positively curved reaction zones concentrating at the leading edge, see black solid line in figure 7, but (ii) does not seem to be appropriate for the latter rate $\dot{\omega}_T$ in lean hydrogen-air turbulent flames. Indeed, the highest heat release rate is reached in negatively curved reaction zones, see figures 19 and 20(b), but the probability of finding such zones is low at low $\langle c\rangle$ for purely topological reasons, see red dashed line in figure 7.

Nevertheless, the leading point concept could still be useful for indirectly evaluating the heat-release-based U_t^T, as $U_t^T \approx U_t^F$, see figures 1 and 16, as well as table 1. Therefore, to evaluate U_t^T, the concept should be applied to U_t^F. Similarly, the speed S_t of a fully developed turbulent flame may be evaluated either by (i) integrating $\dot{\omega}_{H_2}$ (or $\dot{\omega}_T$) along the normal to the mean flame brush or (ii) by exploring the speed of the leading edge of the flame brush. Both problems (evaluation of U_t^T or evaluation of S_t) could hypothetically be solved by selecting one of two alternative methods, but a more elaborated method (i.e., the leading point concept and a constraint of $U_t^T \approx U_t^F$) should be adopted to evaluate U_t^T due to the lack of models with documented capabilities for

directly predicting a significant increase in U_t^T with decreasing Lewis number in lean hydrogen-air turbulent flames.

4. Concluding remarks

The analyzed DNS data show that significant influence of differences in molecular transport coefficients of reactants and/or heat on burning rate in highly turbulent premixed flames does not contradict mitigation of the influence of these differences on the conditioned profiles of various local flame characteristics (equivalence ratio, species concentrations, etc.), sampled from the entire flame brush. The DNS results plotted in figures 1 and 2-6 indicate that both turbulent burning velocities and the conditioned profiles of T, ϕ, $\dot{\omega}_{H_2}$, $\dot{\omega}_T$, and Y_H, sampled at $\langle c \rangle = 0.1 \pm 0.02$ are significantly affected by Le, whereas the conditioned profiles of the same quantities, sampled from the middle of the C-flame brush, are associated with $Le = 1$. This observation not only shows that differences in molecular transport coefficients of reactants and/or heat play a more important role at the leading edge of a mean turbulent flame brush, e.g., because reaction zones are highly curved in the vicinity of the leading edge, but also implies that the turbulent burning velocities are controlled by processes localized to the leading edge, in line with the leading point concept. The special role played by the leading edge in premixed turbulent combustion is further supported by DNS data obtained in cases C1/H2 (Lewis numbers are equal to unity for all species with the exception of H_2) and C1/H (Lewis numbers are equal to unity for all species with the exception of H). In these two cases, differential diffusion phenomena are more pronounced at the leading and trailing edges, respectively, but turbulent burning velocity is significantly larger in the former case.

To be sure that (i) molecular transport is dominated by turbulent mixing and (ii) a regime of distributed burning is reached, conditioned profiles of equivalence ratio, species concentrations, etc. should be explored not only for the entire flame brush, but also for its leading and trailing zones separately. The present authors are not aware on a study where mitigation of the influence of molecular transport on conditioned profiles of equivalence ratio, fuel consumption or heat release rate, etc. is documented in the leading zone of a mean flame brush. Accordingly, phenomena associated with differences in molecular transport coefficients of reactants and/or heat appear to be of importance at Karlovitz numbers significantly higher than commonly believed. Nevertheless, dependencies of turbulent burning velocities on Ka, reported by Aspden et al. (2019, figure 4c), imply that the distributed burning regime was reached in that DNS study at $Ka = O(10^3)$.

Finally, the present study calls for exploring the following issues:

- Since local flow characteristics vary significantly on the scale of the laminar flame, how perturbations of reaction zones by small-scale turbulent eddies could be characterized in the case of $Ka \gg 1$?
- Is there the maximum possible (for specific mixture composition, temperature, and pressure) fuel consumption rate? Can this extreme rate be reached in differently perturbed reaction zones? Are highly strained planar stationary laminar premixed flames appropriate for estimating this extreme rate?

Acknowledgments

ANL gratefully acknowledges the financial support by the Combustion Engine Research Center (CERC). Other authors have been supported in part by NSFC (Grant Nos. 91752201 and 51976088), the Shenzhen Science and Technology Program (Grant No. KQTD2 0180411143441009), Department of Science and Technology of Guangdong

Province (Grant Nos. 2019B21203001 and 2020B1212030001), and by project no. L CH-2019011 under the Joint Program of Shenzhen Clean Energy Research Institute and SUSTech through contract CERI-KY-2019-003.

Declaration of Interests. The authors report no conflict of interest.

REFERENCES

Abdel-Gayed, R. G., Bradley, D., Hamid, M. N. & Lawes, M. 1984a Lewis number effects on turbulent burning velocity. *Proc. Combust. Inst.* **20**, 505–512.

Abdel-Gayed, R. G., Al-Khishali, K. J. & Bradley, D. 1984b Turbulent burning velocities and flame straining in explosions. *Proc. R. Soc. London* **A391**, 393–414.

Abdelsamie, A., Fru, G., Oster, T., Dietzsch, F., Janiga, G. & Thévenin, D. 2016 Towards direct numerical simulations of low-Mach number turbulent reacting and two-phase flows using immersed boundaries. *Comput. Fluids* **131**, 123–141.

Aldushin, A. P., Zel'dovich, Ya. B. & Khudyaev, S. I. 1979. Numerical investigation of flame propagation in a mixture reacting at the initial temperature. *Combust. Explos. Shock Waves* **15**, 705–710.

Amato, A., Day, M., Cheng, R. K., Bell, J. & Lieuwen, T. 2015a Leading edge statistics of turbulent, lean, H_2-air flames. *Proc. Combust. Inst.* **35**, 1313–1320.

Amato, A., Day, M., Cheng, R. K., Bell, J., Dasgupta, D. & Lieuwen, T. 2015b Topology and burning rates of turbulent, lean, H_2/air flames. *Combust. Flame* **162**, 4553–4565.

Aspden, A. J., Day, M. S. & Bell, J. B. 2011a Turbulence-flame interactions in lean premixed hydrogen: transition to the distributed burning regime. *J. Fluid Mech.* **680**, 287–320.

Aspden, A. J., Day, M. S. & Bell, J. B. 2011b Lewis number effects in distributed flames. *Proc. Combust. Inst.* **33**, 1473–1480.

Aspden, A. J., Day, M. S. & Bell, J. B. 2015 Turbulence-chemistry interaction in lean premixed hydrogen combustion. *Proc. Combust. Inst.* **35**, 1321–1329.

Aspden, A. J., Day, M. S. & Bell, J. B. 2016 Three-dimensional direct numerical simulation of turbulent lean premixed methane combustion with detailed kinetics. *Combust. Flame* **165**, 266–283.

Aspden, A. J., Day, M. S. & Bell, J. B. 2019 Towards the distributed burning regime in turbulent premixed flames. *J. Fluid Mech.* **871**, 1–21.

Bilger, R. W., Pope, S. B., Bray, K. N. C. & Driscoll, J. F. 2005 Paradigms in turbulent combustion research. *Proc. Combust. Inst.* **30**, 21–42.

Bradley, D., Lau, A. K. C. & Lawes, M. 1992 Flame stretch rate as a determinant of turbulent burning velocity. *Phil. Trans. R. Soc. London A* **338**, 359–387.

Bradley, D., Gaskell, P. H., Gu, X. J. & Sedaghat, A. 2005 Premixed flamelet modelling: factors influencing the turbulent heat release rate source term and the turbulent burning velocity. *Combust. Flame* **143**, 227–245.

Bray, K. N. C. & Cant, R. S. 1991 Some applications of Kolmogorov's turbulence research in the field of combustion. *Proc. R. Soc. London A* **434**, 217–240.

Carlsson, H., Yu, R. & Bai, X. S. 2014 Direct numerical simulation of lean premixed CH_4/air and H_2/air flames at high Karlovitz numbers. *Int. J. Hydrogen Energy* **39**, 20216–20232.

Carroll, P. L. & Blanquart, G. 2014 The effect of velocity field forcing techniques on the Karman–Howarth equation. *J. Turbul.* **15**, 429–448.

Chakraborty, N. & Cant, R. S. 2011 Effects of Lewis number on flame surface density transport in turbulent premixed combustion. *Combust. Flame* **158**, 1768–1787.

Chakraborty, N. & Lipatnikov, A. N. 2013a Effects of Lewis number on conditional fluid velocity statistics in low Damköhler number turbulent premixed combustion: a Direct Numerical Simulation analysis. *Phys. Fluids* **25**, 045101.

Chakraborty, N. & Lipatnikov, A. N. 2013b Conditional velocity statistics for high and low Damköhler number turbulent premixed combustion in the context of Reynolds Averaged Navier Stokes simulations. *Proc. Combust. Inst.* **34**, 1333-1345.

Chakraborty, N., Konstantinou, I. & Lipatnikov, A. N. 2016 Effects of Lewis number on vorticity and enstrophy transport in turbulent premixed flames. *Phys. Fluids* **28**, 015109.

Class, A. G., Matkowsky, B. J. & Klimenko, A. Y. 2003 A unified model of flames as gasdynamic discontinuities. *J. Fluid Mech.* **491**, 11–49.

Clavin P. & Liñán, A. 1984 Theory of Gaseous Combustion. In *Nonequilibrium Cooperative Phenomena in Physics and Related Fields* (ed. M. G. Velarde), pp. 291–338. NATO ASI Series (Series B: Physics), Springer, Boston, MA.

Daniele, S., Jansohn, P., Mantzaras, J. & Boulouchos, K. 2011 Turbulent flame speed for syngas at gas turbine relevant conditions. *Proc. Combust. Inst.* **33**, 2937–2944.

Dasgupta, D., Sun, W., Day, M. & Lieuwen, T. 2017 Effect of turbulence-chemistry interactions on chemical pathways for turbulent hydrogen-air premixed flames. *Combust. Flame* **176**, 191–201.

Dave, H. L., Mohan, A. & Chaudhuri, S. 2018 Genesis and evolution of premixed flames in turbulence. *Combust. Flame* **196**, 386–399.

Driscoll, J.F., Chen, J. H., Skiba, A. W., Carter, C. D., Hawkes, E. R. & Wang, H. 2020 Premixed flames subjected to extreme turbulence: some questions and recent answers. *Prog. Energy Combust. Sci.* **76**, 100802.

Ebert, U. & van Saarlos, W. 2000 Front propagation into unstable states: universal algebraic convergence towards uniformly translating pulled fronts. *Physica D* **146**, 1–99.

Goodwin, D., Malaya, N., Moffat, H. & Speth, R. 2009 Cantera: An object-oriented software toolkit for chemical kinetics, thermodynamics, and transport processes. Caltech, Pasadena, CA.

Gruber, A., Bothien, M. R., Ciani, A., Aditya, K., Chen, J. H. & Williams, F. A. 2021 Direct Numerical Simulation of hydrogen combustion at auto-ignitive conditions: Ignition, stability and turbulent reaction-front velocity. *Combust. Flame* **229**, 111385.

Karpov, V. P. & Sokolik, A. S. 1961 Ignition limits in turbulent gas mixtures. *Proc. Acad. Sci. USSR, Phys. Chem.* **141**, 866–869.

Karpov, V. P. & Severin, E. S. 1980 Effects of molecular-transport coefficients on the rate of turbulent combustion. *Combust. Explos. Shock Waves* **16**, 41–46.

Karpov, V. P., Lipatnikov A. N. & Zimont, V. L. 1996 A test of an engineering model of premixed turbulent combustion. *Proc. Combust. Inst.* **26**, 249–257.

Kelley, A. P., Bechtold, J. K. & Law, C. K. Premixed flame propagation in a confining vessel with weak pressure rise. *J. Fluid Mech.* **691**, 26–51.

Kéromnès, A., Metcalfe, W. K., Heufer, K. A., Donohoe, N., Das, A. K., Sung, C.-J., Herzler, J., Naumann, C., Griebel, P., Mathieu, O., Krejci, M. C., Petersen, E. L., Pitz, W. J. & Curran, H. J. 2013 An experimental and detailed chemical kinetic modeling study of hydrogen and syngas mixture oxidation at elevated pressures. *Combust. Flame* **160**, 995–1011.

Kha, K. Q. N., Robin, V., Mura, A. & Champion, M. 2016 Implications of laminar flame finite thickness on the structure of turbulent premixed flames. *J. Fluid Mech.* **787**, 116–147.

Kido, H., Kitagawa, T., Nakashima, K. & Kato, K. 1989 An improved model of turbulent mass burning velocity. *Memoirs Faculty Eng. Kyushu Univ.* **49**, 229–247.

Kim, S. H. 2017 Leading points and heat release effects in turbulent premixed flames. *Proc. Combust. Inst.* **36**, 2017–2024.

Klimov, A. M. 1963 Laminar flame in a turbulent flow. *Zh. Prikl. Mekch. Tekhn. Fiz.* **4**, No. 3, 49–58.

Kolmogorov, A. N., Petrovsky, E. G. & Piskounov, N. S. 1937 A study of the diffusion equation with a source term and its application to a biological problem. *Bjul. MGU Section A* **1(6)**, 1–26.

Kuznetsov, V. R. & Sabelnikov, V. A. 1990 *Turbulence and Combustion*, Hemisphere Publ. Corp.

Lapointe, S. & Blanquart, G. 2016 Fuel and chemistry effects in high Karlovitz premixed turbulent flames. *Combust. Flame* **167**, 394–307.

Lapointe, S., Savard, B. & Blanquart, G. 2015 Differential diffusion effects, distributed burning, and local extinction in high Karlovitz premixed flames. *Combust. Flame* **162**, 3341–3355.

Lee, H. C., Dai, P., Wan, M. & Lipatnikov, A. N. 2021a A DNS study of extreme and leading points in lean hydrogen-air turbulent flames - part I: Local thermochemical structure and reaction rates. *Combust. Flame*, in press.

Lee, H. C., Dai, P., Wan, M. & Lipatnikov, A. N. 2021b A DNS study of extreme and leading points in lean hydrogen-air turbulent flames - part II: Local velocity field and flame topology. *Combust. Flame*, in press.

Lipatnikov, A. 2012 *Fundamentals of Premixed Turbulent Combustion*. CRC Press.

Lipatnikov, A. N. & Chomiak, J. 1998 Lewis number effects in premixed turbulent combustion and highly perturbed laminar flames. *Combust. Sci. Technol.* **137**, 277–298.

Lipatnikov, A. N. & Chomiak, J. 2005 Molecular transport effects on turbulent flame propagation and structure. *Prog. Energy Combust. Sci.* **31**, 1–73.

Lipatnikov, A. N., Chakraborty, N. & Sabelnikov, V. A. 2018 Transport equations for reaction rate in laminar and turbulent premixed flames characterized by non-unity Lewis number. *Int. J. Hydrogen Energy* **43**, 21060–21069.

Lundgren, T. 2003 Linearly forced isotropic turbulence. Tech. Rep., Minnesota University of Minneapolis.

Matalon, M. & Matkowsky, B. J. 1982 Flames as gas dynamic discontinuities. *J. Fluid Mech.* **124**, 239–260.

Nilsson, T., Carlsson, H., Yu, R. & Bai, X.-S. 2018 Structures of turbulent premixed flames in the high Karlovitz number regime – DNS analysis. *Fuel* **216**, 627–638.

Pelcé, P. & Clavin, P. 1982 Influence of hydrodynamics and diffusion upon the stability limits of laminar premixed flames. *J. Fluid Mech.* **124**, 219–237.

Peters, N. 2000 *Turbulent Combustion*. Cambridge University Press.

Poinsot, T. & Veynante, D. 2005 *Theoretical and Numerical Combustion*, 2nd edn. Edwards.

Rieth, M., Gruber, A., Williams, F. A. & Chen, J. H. 2021 Enhanced burning rates in hydrogen-enriched turbulent premixed flames by diffusion of molecular and atomic hydrogen. *Combust. Flame*, accepted.

Rosales, C. & Meneveau, C. 2005 Linear forcing in numerical simulations of isotropic turbulence: Physical space implementations and convergence properties. *Phys. Fluids* **17**, 095106.

Sabelnikov, V. A. & Lipatnikov, A. N. 2013 Transition from pulled to pushed premixed turbulent flames due to countergradient transport. *Combust. Theory Modelling* **17**, 1154–1175.

Sabelnikov, V. A. & Lipatnikov, A. N. 2015 Transition from pulled to pushed fronts in premixed turbulent combustion: theoretical and numerical study. *Combust. Flame* **162**, 2893–2903.

Sabelnikov, V. A., Petrova, N. N. & Lipatnikov, A. N. 2016 Analytical and numerical study of travelling waves using the Maxwell-Cattaneo relaxation model extended to reaction-advection-diffusion systems. *Phys. Rev. E* **94**, 042218.

Sabelnikov, V. A., Lipatnikov, A. N., Nishiki, S., Dave, H. L., Hernández-Pérez, F. E., Song, W. & Im, H.G. 2021 Dissipation and dilatation rates in premixed turbulent flames. *Phys. Fluids* **33**, 035112.

Savard, B. & Blanquart, G. 2014 An a priori model for the effective species Lewis numbers in premixed turbulent flames. *Combust. Flame* **161**, 1547–1557.

Savard, B., Bobbit, B. & Blanquart, G. 2015 Structure of a high Karlovitz n-C_7H_{16} premixed turbulent flame. *Proc. Combust. Inst.* **35**, 1377–1384.

van Saarloos, W. 2003 Front propagation into unstable states. *Phys. Reports* **386**, 29–222.

Venkateswaran, P., Marshall, A., Shin, D. H., Noble, D., Seitzman, J. & Lieuwen, T. 2011 Measurements and analysis of turbulent consumption speeds of H_2/CO mixtures. *Combust. Flame* **158**, 1602–1614.

Venkateswaran, P., Marshall, A., Seitzman, J. & Lieuwen, T. 2013 Pressure and fuel effects on turbulent consumption speeds of H_2/CO blends. *Proc. Combust. Inst.* **34**, 1527–1535.

Venkateswaran, P., Marshall, A., Seitzman, J. & Lieuwen, T. 2015 Scaling turbulent flame speeds of negative Markstein length fuel blends using leading points concepts. *Combust. Flame* **162**, 375–387.

Veynante, D. & Vervisch, L. 2002 Turbulent combustion modeling. *Prog. Energy Combust. Sci.* **28**, 193–266.

Verma, S., Monnier, F. & Lipatnikov, A. N. 2021 Validation of leading point concept in RANS simulations of highly turbulent lean syngas-air flames with well-pronounced diffusional-thermal effects. *Int. J. Hydrogen Energy* **46**, 9222–9233.

Williams, F. A. 2000 Progress in knowledge of flamelet structure and extinction. *Prog. Energy Combust. Sci.* **26**, 657–682.

Wiseman, S., Rieth, M., Gruber, A., Dawson, J. R. & Chen, J. H. 2021 A comparison of the blow-out behavior of turbulent premixed ammonia/hydrogen/nitrogen-air and methane-air flames. *Proc. Combust. Inst.* **38**, 2869–2876.

Wohl, K. & Shore, I. 1955 Experiments with butane-air and methane-air flames. *Ind. Eng. Chem.* **47**, 828–834.

Wu, M. S., Kwon, A., Driscoll, J., and Faeth, G. M. 1990 Turbulent premixed hydrogen/air flames at high Reynolds numbers. *Combust. Sci. Technol.* **73**, 327–350.

Yang, S., Saha, A., Liang, W., Wu, F. & Law, C. K. 2018 Extreme role of preferential diffusion in turbulent flame propagation. *Combust. Flame* **188**, 498–504.

Yeung, P. & Pope, S. 1989 Lagrangian statistics from direct numerical simulations of isotropic turbulence. *J. Fluid Mech.* **207**, 531–586.

Zel'dovich, Ya. B. 1980 Regime classification of an exothermic reaction with nonuniform initial conditions. *Combust. Flame* **39**, 211–214.

Zel'dovich, Ya. B. & Frank-Kamenetskii, D. A. 1938 A theory of thermal flame propagation. *Acta Physicochemia URSS*, **9**, 341–347.

Zel'dovich, Ya. B., Barenblatt, G. I., Librovich, V. B. & Makhviladze, G. M. 1985 *The Mathematical Theory of Combustion and Explosions*. Consultants Bureau.

Zhang, W., Wang, J., Yu, Q., Jin, W., Zhang, M. & Huang, Z. 2018 Investigation of the fuel effects on burning velocity and flame structure of turbulent premixed flames based on leading points concept. *Combust. Sci. Technol.* **190**, 1354–1376.